MODELING OF DIELECTRIC ELASTOMER ACTUATORS WITH A CONICAL SHAPE

Niloufarsadat Nouhi

A thesis
in
The Department
of
Mechanical, Industrial and Aerospace Engineering

Presented in Partial Fulfillment of the Requirements
For the Degree of Master of Applied Science
Concordia University
Montréal, Québec, Canada

December 2021

Concordia University
School of Graduate Studies

This is to certify that the thesis prepared

By: **Niloufarsadat Nouhi**

Entitled: **Modeling of dielectric elastomer actuators with a conical shape**

and submitted in partial fulfillment of the requirements for the degree of

Master of Applied Science

complies with the regulations of this University and meets the accepted standards with respect to originality and quality.

Signed by the final examining commitee:

Dr. Youmin Zhang _____ Chair

Dr. Youmin Zhang _____ Examiner

Dr. Lan Lin _____ Examiner

Dr. Chun-Yi Su _____ Supervisor

Approved by _____

Dr.Martin D. Pugh Chair of Department or Graduate Program Director

_____

Dr. Mourad Debbabi, Interim Dean

Faculty of Engineering and Computer Science

Abstract

Modeling of dielectric elastomer actuators with a conical shape

Niloufarsadat Nouhi

Dielectric elastomer actuators (DEAs) have received a lot of attention in the last decade due to their outstanding actuation strain, high energy density, high degree of freedom, electromechanical coupling and low price. However, modelling of dielectric elastomer actuators is complicated because of time-dependent viscoelasticity, complex geometry, electromechanical coupling and material nonlinearity. For these reasons, just a few research results focusing on modeling of the DEAs have been published.

In this research, taking into account the influence of viscoelasticity, we present a physical and phenomenal based model to characterize the behaviour of a conical DEA made of polydimethylsiloxane. The nonequilibrium thermodynamic framework is used to characterize the mechanical coupling of DEA. Also free energy and viscoelastic characteristics of DEA are described using the Gent model and the generalized Kelvin model, respectively.

The differential evolution approach is used to find the model parameters based on the experimental data. The model's validity and generalization are proved by comparing experimental results with model predictions, for both different driving input frequencies and amplitudes. The experimental results demonstrate a high level of agreement with developed model.

Acknowledgments

First of all, I want to reach out to my supervisor and professor, Dr. Chun-Yi Su, to express my deepest gratitude for all the support and guidance he has given me during my Master studies, you are truly the best professor in the world. Despite my slow start he gave me the motivation to find myself and believe in my abilities. He has taught me not only knowledge but things for the long run. Thank you for the opportunity and patients. I can not show my gratitude enough with words. I can only say from the bottom of my heart THANK YOU and will never forget all you have thought me.

I would like to show my gratitude to Dr. Yawu Wang who have inspired me with his great ideas and consistently provided me with experimental tests. Finishing my thesis during the pandemic without his support would have been very hard.

I would like to give a special thanks to Dr. Wenjun Ye for their generous advices and support. He has helped more than I asked, his unconditional help will never be forgotten.

Last but not least, I would like to thank my family for their support financially and emotionally, and my partner who have been by my side in ups and downs, and kept me motivated in my studies and my life. The only thing that kept me going is to make them proud. They have always encouraged me to follow my dreams. I am truly blesses to have you.

Contents

List of Figures

List of Tables

Chapter 1

Introduction

1.1 Objective of the thesis

Since the rapid development of soft robotics, the dielectric elastomer actuators (DEAs) have become more popular due to their overall low cost, attractive inherent characteristics include high energy density, fast response speed, high efficiency and high deformability. However, DEAs have shown viscoelastic behaviour, which makes them very nonlinear and time-dependent.

The majority of the previous studies developed some static or quasi-static models to explicate the material behavior of DEA with simple configurations. However, the dynamic behavior of DEA has been neglected due to some challenges such as nonlinear viscoelasticity, electromechanical coupling and complex shape.

Concerning the DEA with complex shape, this study offers a phenomenal model that can accurately characterize viscoelasticity and motion responses of a conical DEA . First we use the nonequilibrium thermodynamics theory to describe the electromechanical behviour of DEA. Then, the Gent model and the generalized Kelvin model have been used to describe the free energy and viscoelastic behaviour of the DEAs, respectively. Finally, the experimental identification and validation procedure performed to test the effectiveness of the model over different voltages and frequencies.

1.2 Thesis overview

This thesis consists of 5 chapters, which are organized as follows:

- ❒ Chapter 1 is delegated to introduce the idea of modeling of DEA.
- ❒ Chapter 2 reviews previous studies, including review of the soft robots and working priciple of dielectric elastomer actuator and discuss the state of the art.
- ❒ Chapter 3 develops a dynamic model for a conical dielectric elastomer actuator based on the nonequilibrium thermodynamic.
- ❒ Chapter 4, the experimental setup and model identification are conducted. The theoretical and experimental comparisons are discussed as well in this chapter. Finally the effectiveness of the model is validated by the experiment test.
- ❒ Chapter 5, concludes all results and addresses future works.

Chapter 2

Literature review

2.1 Soft robotics

Nowadays, soft robotics is becoming an increasingly important field due to its growing applications beyond industrial automation into areas such as health care, biomedical and human robots [3]. Therefore the development of soft robots is necessary; these developments includes some aspects such as materials, actuators, design, modelling and applications [4]. From the material perspective, we can categorize robots into hard or soft. Traditionally, engineers preferred to manufacture robots with rigid materials, like aluminum, metal and steel, because of high stiffness characteristics, which allow them to generate massive forces. Also, the structure of conventional robots has provided engineers with precise control and predictable behaviour [5, 6, 7].

However, the limited degrees of freedom and rigid structure of hard robots cause their movement to be more challenging when interacting with humans and nature. Hence, scientists by inspiration of biological mechanisms, have invented soft robots using flexible joints and soft materials [7, 8]. Soft materials have larger deformations and flexible structure which allow robots to safely move and be more compatible and adaptable when maneuvering in different spaces, such as interacting with humans and nature [9]. These innovations have made significant development on applications of robots as you can see in Figure 1. One of the important applications of soft materials is soft actuator.

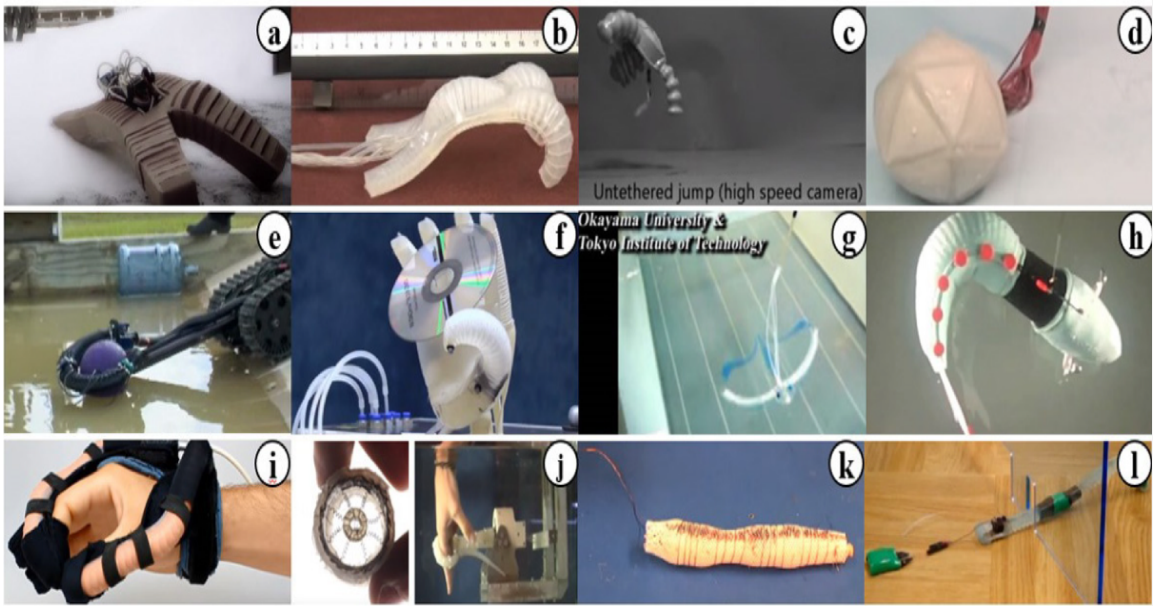

Figure 1: applications of soft robots

2.2 Actuators

During the past decade, many researchers have studied various soft robots that use different actuation technologies and mechanisms [10]. An actuator is a mechanical device that converts input energy to mechanical output energy. In contrast to the traditional robots actuated with rigid motors, rotational and linear actuation systems, most soft robots are actuated in two ways: the tendon-driven actuation and soft smart materials actuation [11].

2.2.1 Tendon-driven actuation

The first category, tendon-driven actuation, also known as continuum robot has a multiple joints which driven by a cable that passes through the joints resulting in infinite degrees of freedom and continuum deformation Figure 2. Also they can deliver a controlled force to deform the segment in a desired way, such as tension cables actuators. The practical applications of this kind of robots are existed in medical and rescue fields [11]. However, such soft robots primarily employs conventional motors and solid mechanisms, leading to not being completely soft robots. For example in [12] , a tendon-driven manipulator made of silicone inspired by the octopus arm is

presented, reader may refer to [13] for more details about this kind of robots.

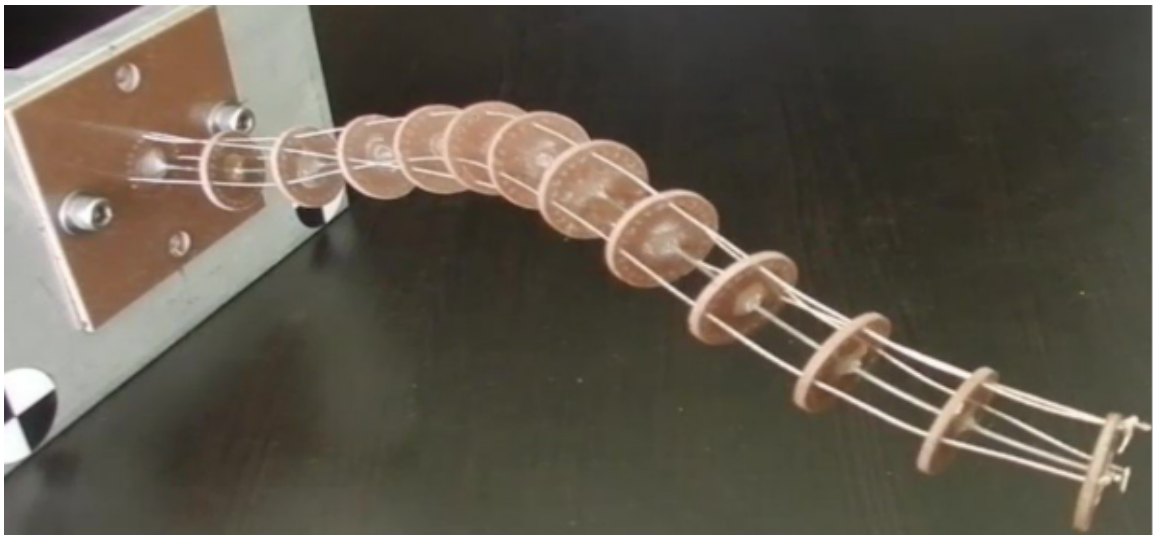

Figure 2: A tendon-driven robot

2.2.2 Smart materials actuation

The second group is smart materials actuation Figure 3. In contrast to continuum robots, soft smart materials actuation has the ability to convert energy directly. There are two common types of soft smart materials actuations include fluidic actuators (such as pneumatic and hydrolic) and intelligent material actuators (electroactive polymers (EAPs)), which are popular because of the advantages of light weight and low cost [5, 14, 15] .

Figure 3: A smart material robot

Recently, EAPs have significantly been noticed by researchers because of their potential uses and outstanding features. The electro-active polymer technology has made actuators which are lightweight, energy efficient, and scalable. Also, EAPs can mimic the properties of biological muscle, when stimulated by the input energy; they show high fracture, large actuation strain and inherent vibration damping[16]. Considering the various stimuli processes, EAPs can generally divide into two major groups based on their methods of actuations: ionic EAPs and electronic EAPs.

Ionic EAPs can generally respond to different external stimuli; the most commonly used are chemical and electrolytic reactions that require low voltage to have a large bending displacement. However, the main issues of these systems are their slow actuation rates. A detailed description can be found in [17].

The electronic EAPs are polymer with polar side groups. They have the advantages of high energy density, rapid response time (in the range of milliseconds) and the larger force compared to the ionic type. The typical sorts of EAPs is dielectric elastomer (DE) which is mostly implemented in practical applications [18, 19]. In the next part, we present more detail about dielectric elastomer actuator (DEA).

2.3 Dielectric elastomer actuator

Compare to other smart materials, dielectric elastomer (DE) has shown attractive characteristics, which have made them very popular in application of soft robots. Characteristics, such as high deformation, high energy density, high electromechanical-coupling efficiencies, low cycling hysteresis, lightweight and low costs [20]. Also, DEAs are able to both actuate and generate power in different geometries [1].

2.3.1 DEAs applications

Nowadays, DEAs are used to develop soft robots that can carry out sophisticated manipulation tasks. The flexible structure of DEAs, allow them to deal with uncertainty in a manner comparable to the natural organisms which make them safe for human interactions and complex environment. Also, their resemblance to biological

muscles have made scientists to use them as an artificial muscle in biomedical applications [21]. The followings present some of the applications of DEAs as grippers and humanoid robots.

Grippers

One of the most challenging problems in robotics is gripping objects with complex shapes. Researchers are looking into DEAs as a possible answer to this problem. With a DEA, the inherent flexibility allows for close contact between an object and a gripper while maintaining an effective grabbing arrangement. Also DEA's lightweight and high energy density is critical to developing a high weight ratio of gripper mass to grasping capability. Different varieties of DE grippers have been produced with diverse configurations based on a simple working concept and large actuation strain of the DEA.

G. Kofod et al [22] introduced DE grippers in 2007, based on a dielectric elastomer minimum energy structure. In which a pre-stretched DE is laminated to a flexible plastic frame to create an out-of-plane arrangement When the pre-stretched DE's tension shrinks its own structure, releasing elastic energy. Then, a portion of the released energy is retained in the flexible plastic frame, resulting in bending. The tension of the DE lowers as voltage is added to it, and the entire structure opens up enough to grip a target object.

Humanoid robots

DEA is one of the promising actuation technologies which can mimic real human muscles in terms of appearance, actuation strain, actuation density and response time. Over the past two decades, several studies have been spent to use DEAs as humanoid robots.

One of the importatnt part of humanoid robot is visual system. In [23], a bioinspired actuation mechanism was proposed for the construction of simple bioinspired actuation mechanisms to mimic the eyeballs of an android robotic face. The actuators' configuration and functionality were designed to resemble those of rectus-type human ocular muscles. They also developed a buckling DEA with constrained boundaries

to achieve the maximum displacement for actuation of robotic eyeball mechanism [24].

In another recent study, artificial muscles have been built utilising DEAs to drive a robotic jaw . The human jaw movements are driven by several groups of muscles including temporalis, masseter, digastric, medial pterygoid muscles and lateral pterygoid muscles. In order to mimic the real human jaw movement, the two DEAs are installed on a robotic skull, at the same positions to those of the masseters in a human jaw. The linear planar DEAs can provide precise and controllable deformations of varied amplitudes and frequencies, which are comparable to real-world human jaw movement capabilities such as talking. The fibres are found to significantly improve the actuator's performance. Experiments reveal that the jaw's highest vertical displacement corresponds to the real human jaw's maximum movement. This research adds to the development of a viscoelastic actuator with controllable motions and massive voltage-induced deformation. A viscoelastic nonlinear dynamic model for the jaw is also built to improve control effect or accuracy, and the nonlinear feedforward controller constructed based on the model is capable of monitoring desired trajectories and emulating human jaw actions in a speech with high accuracy [25].

2.3.2 DEAs configuration

Based on the different configurations, dielectric elastomers can be employed in various applications, from industrial to medical, for example, tuning stages for soft diffractive grating [26, 27], tunable organic lasers [28], stretchable electronics [29], energy harvesters [30, 31, 32], soft computers and soft motors [33, 34], human-machine interface structural health monitoring for buildings [35, 36].

The functioning, capability, and reliability of actuators made of DEs are highly dependent on actuator configuration. Different boundary constraints result in various configurations and modes of deformation. Therefore, DEAs can be configured in many ways, including planar (in-plane, framed, diaphragm), rolled (tubular, cylindrical), laminated (stacked or folded), conical and so on [22, 37, 38, 39]. As an illustration, Figure 4 presents some typical configurations of DEAs [1]. Generally, DE films can be stretched over a frame or rolled into a scroll, in which they can be configured to make in-plane or out-of-plan deformation to achieve muscle-like behavior for thin elastomer or memberane.

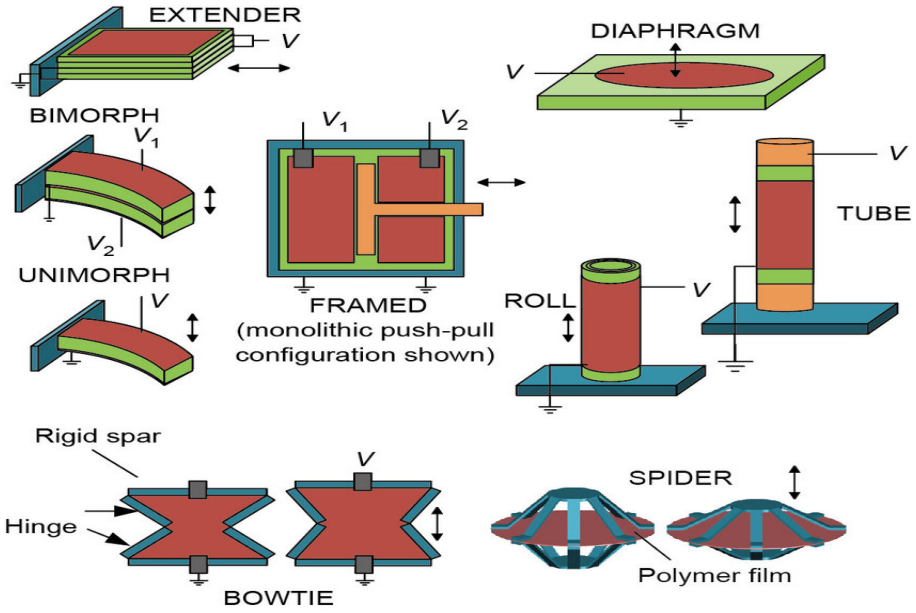

Figure 4: Diffrent configurationd of DEAs (adopted from [1]).

Diaphragm

A diaphragm actuator is typically made up of a circular membrane that is expanded in both directions and has its boundary restricted by a rigid frame that can produce out of plane deformation [40]. This type of configuration is employed in pumps, loudspeakers, controllable surface roughness for aerodynamics [41]. Follador et al. recently created a new suction cup employing DEs that was able to produce up to 6 kPa of pressure in water with a fast response, inspired by octopus suckers [42].

Rolled

Tube DEs are rolled actuators with one fixed end that can actuate in both axial and radial directions, used in peristaltic pumps [43]. When a DE tube exposes an external field, a reduction in thickness accompanied by elongation in the axial can be observed. Moreover, DE structures or devices with various configurations have multi-degrees of freedom upon actuation. Antagonistically driven linear actuator (ANTLA) developed by Choi et al. also investigates the concept of varied configurations to achieve multiple degrees of freedom [44].

Laminated

Stacking or laminated configurations consist of several layers of dielectric elastomer, which offer linear contractile actuation and provide larger forces in the thickness direction compare to thin films. Carpi et al. [45] devised this new configuration, which consists of two helical compliant electrodes separated by an elastomeric insulator [46]. The stacked configuration is ideal for compact, versatile, and compliant systems, as well as noise-free actuation [6, 37]. However, the non-uniform distribution of strain along the length of stacking actuators with flexible electrodes is the key disadvantage of this multi-layer design.

Conical

Among various configurations in dielectric elastomer actuators, conical DEA are one of the most popular actuators for their multi- degree-of-freedom design, which allows them to actuate more than one degree of freedom [47]. For this reason, we are going to use the conical configuration.

2.3.3 DEs material

One of the most important aspects of DEAs is DE material selection. DE materials should have a low elastic modulus, low viscosity, high dielectric constant, and strong electrical breakdown strength to improve DEA performance. Currently, polyacrylate and polydimethylsiloxane are the two most popular DE materials [48].

Many researchers [49, 50] employ VHB, (3M VHB4905/4910), a kind of polyacrylate material manufactured by 3M in the United States, to make the DEA because it is readily available and inexpensive. Also, VHB have lower DE constants than polydimethylsiloxane or PDMS , requiring greater electrical fields to create high strain [51].

On the other hand, VHB have a higher viscosity than PDMS, which make PDMS are better suited to high-frequency applications. They can be employed to make dielectric elastomers actuators (DEAs), and their use in actuators and sensors has gotten much attention.

Unfortunately, there are few researchers exploring the dynamic characteristics of the DEA based on PDMS [2, 48]. In this study we choose the PDMS to fabricate a conical DEA as an illustration for the further investigation.

2.3.4 Challenges

Despite these promising applications, there are still major challenges between the developed robots and real biological examples. These technical challenges make the applications of DEA limited in complex soft robots. For instance, how to model the actuator with dissipative and nonlinear behaviour of DEs such as the inherent viscoelasticity, creep and time dependent performance of dielectric elastomers.

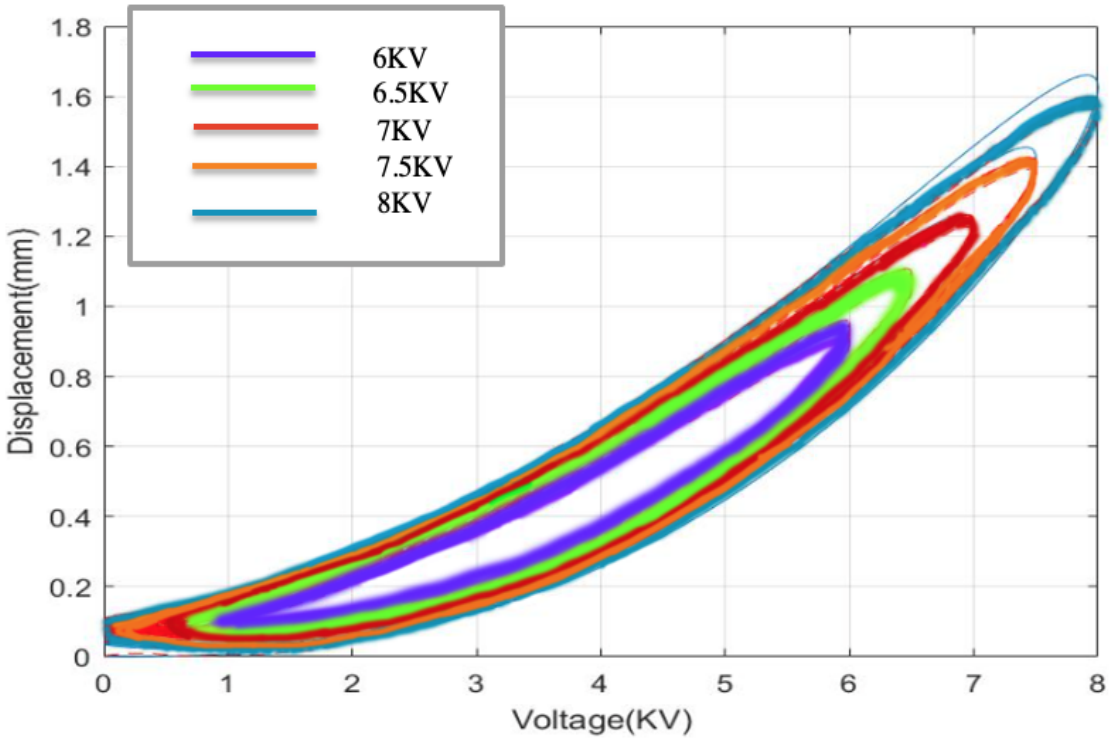

Figure 5: The graph of behaviour of DEA under the voltage stimuli.

In Figure 5, you can see the plot of input voltage versus output displacement, which is multi valued or for each voltage we have different displacement. Also the dependency of plot one the different amplitudes driving voltage is obvious. Therefore modelling of this graph is too complicated because of the obvious viscoelasticity.

Inherent viscoelasticity

The dielectric elastomer has a strong nonlinear viscoelasticity, which is a common challenge for DEs. During actuation, viscoelasticity causes an elastomer's internal stress and strain to fluctuate over time, resulting in a time-dependent deformation, creep and relaxation.

Complex geometery

DEAs can be designed in different configurations with complex shapes which make them difficult to analyse the dynamic behavior. For example, for the conical DEA, the actuator geometery is circular which result to dynamic nonlinearities.

2.4 Modeling approaches

In terms of modeling the nonlinear behaviour of DEA, many studies have been developed.

For instance, Suo [20] presented the theory of DEA on the basis of thermodynamics framework for a planar DEA. In 2017, Gu et al., [49] developed a constitutive modeling approach to properly predict the complex viscoelastic phenomenon in a clamped DEA membrane undergoing cyling load and homogenous deformation. In [25] for a DEA experiencing homogenous deformation, A simplified physics based model was proposed to take into account the effect of viscoelasticity, which was then used to design precise controllers.

Concerning DEA with conical configuration, some studies have been developed. For example, a quasi-static analytical model for a conical DEA, based on thermodynamic equilibrium and neo-Hookean material model is developed in [52]. Also, Wang et al., [53], developed a viscoelastic model for a conical dielectric elastomer actuator connected by a spring which undergoes a large out-of-plane inhomogeneous deformation by applying the electro-mechanical loadings.

In 2018, an analytical model [47] based on optimization for a conical DEA with three biassing elements has presented and the goal was to optimise the geometry and pre-stretch ratio of a conical DEA to get the highest work output.

However, in these papers, the DE material has been employed is mostly VHB, because VHB is commonly available. The VHB has a defect of high viscoelasticity. Although, PDMS is a good replace for the VHB. There are few researchers exploring the dynamic characteristics of the DEA based on the PDMS.

Huang [2] has proposed a dynamic model based on nonequilibrium thermodynamics to describe the complex motion characteristics of a conical DEA made of polydimethylsiloxane and taking into account the effects of inertia. The differential evolution algorithm has been used to identify the indeterminate parameters on the basis of the experimental data. Although these studies have made huge development

to model the behaviour of conical DEAs, they mostly used constitutive and neo-Hookean model.

In this study we propose a dynamic model for a conical DEA made of PDMS based on Generalized kelvin model and nonequilibrium thermodynamics. But first, we need to understand the working principle of a DEA to properly characterize the motion and characteristics of DEAs.

2.4.1 Working principle

Basic theories of DEs

DEAs are soft smart materials that deform dramatically and reversibly when exposed to an electric field. A dielectric elastomer actuator typically consists of a thin film of elastic polymer covered on both sides by compliant electrodes that can transduce electrical stimuli to mechanical energy. A difference in voltage between the compliant electrodes causes deformation and polarization on the DEA simultaneously, in which an expansion in the length and compression in thickness occur to keep a constant volume (incompressible) [54]. The DE membrane recovers its original configuration when the voltage is removed.

The basic element of a DE-based transducer is a dielectric elastomer membrane coated with two compliant electrodes on its two surfaces. When exposed to a voltage, the majority of the opposing charges from the power source collect on the compliant electrodes. While a portion of them leak through the membrane due to elastomer defects or impurities. The opposing charges accumulating on the electrodes generate an electric field in the DE, which results in contracts along DEAs thickness and increases in area due to attractive electrostatic forces. Dielectric elastomer is inevitably accompanied by the generation of forces and changes in shape, which can be used to move or deform an object placed on the membrane.

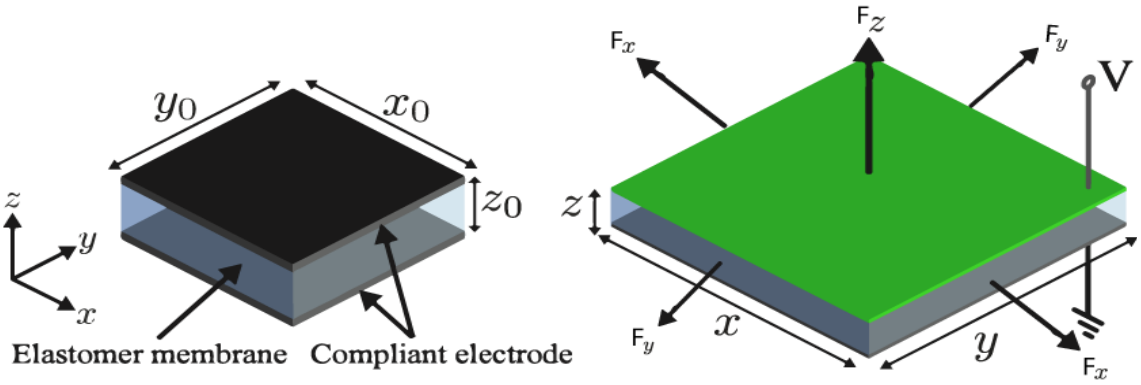

Figure 6: Working principle of a planar DEA.

Dielectric elastomers are believed to be incompressible, implying that the membrane volume remains constant regardless of deformation state.

Consider a planar DEA as shown in Figure 6. The original dimensions of the DE membrane are x_0, y_0, and z_0. When the two electrodes set voltage ϕ, the DE membrane is subjected to forces F_x, F_y, and F_z. Therefore, the new dimension of the membrane become x, y and z, respectively. Then, the elastomer is stretched by $\lambda_x = \frac{x}{x_0}$, $\lambda_y = \frac{y}{y_0}$ and $\lambda_z = \frac{z}{z_0}$, in Cartesian coordinate system. Then if the volume is constant, we obtain:

$$\lambda_x \lambda_y \lambda_z = 1 \tag{1}$$

Ideal DEA

The behaviour of dielectric elastomers is considered to be well described by using idealisation. According to experimental findings in [21, 55], the permittivity ε of various DEs is practically constant throughout deformation. As a result, the true electric displacement, D, and true electric field, E, have a relationship [56].

$$D = \varepsilon E \tag{2}$$

2.4.2 Linear electromechanical modeling

In 2000, Pelrine and Kornbluh created the first physical model to explain the electromechanical actions of DEAs [57]. They discovered that the Maxwell stress causes electromechanical transduction effects in DEs, in which the electrostatic pressure or the generated stress, also known as Maxwell stress, p, is produced when a voltage applied between the electrodes. p can be expressed as below:

$$p = \varepsilon_0 \varepsilon_r \times E^2 \tag{3}$$

where ε_0 and ε_r are the absolute permittivity and relative permittivity of dielectric elastomers, respectively. While E is the nominal electric field applied. Pelrine and his colleagues have provided a simple method to predict DEA strains by applying Hooke's law to Equation (3).

$$s_z = -p/Y = -\varepsilon_0 \varepsilon_r \cdot E^2/Y \tag{4}$$

where s_z is thickness strain and Y is the elastic modulus relating to the strain. Pelrine's approach mentioned in Equation (3) and Equation (4) is a pioneering and well-known method for understanding and predicting the electromechanical response in the field of DEAs.

However, Pelrine's approach cannot be used to tackle for the large deformation and strong nonlinear behavior of DE. Due to the viscoelasticity of DEs, they show nonlinear behavior which cause Pelrine's method not be enough to characterize DEAs behaviour.

2.4.3 Nonlinear electromechanical modeling

The thermodynamic nonequilibrium framework is one of the most widely used modeling frameworks for analyzing DEA dynamics. In 2010, Suo [20] presented the theory of DEA on the basis of thermodynamics framework. According to nonequilibrium thermodynamics, under an isothermal process, the increase in Helmholtz free energy of a DEA must be less or equal the sum of the work done by external forces and actuation voltages. Based on [20], the Helmholtz free energy G, in Figure 6, is defined as:

$$\delta G \leq F_x \delta x + F_y \delta y + F_z \delta x + \phi \delta Q \tag{5}$$

where, δG is the work done by Helmholtz free energy and $\phi \delta Q$ is the work done by electric charges, in which ϕ is the input voltage and Q is the accumulated electric charge . $F_x \delta x$, $F_y \delta y$ and $F_z \delta z$ are the work done by external forces, which δx, δy and δz are the memberane deformations, respectively (see Figure 6).

Baesd on the definition of the the Helmholtz free energy density in W, is defined as:

$$W = \frac{G}{V} \tag{6}$$

In which, V is the volume of the DEA's membrane. Then by dividing the volume of the DEA's membrane, $l_1 l_2 l_3$ form both sides in Equation (5), and assuming that the DEA has the ideal dielectric elastomer membrane, the free energy density, can be expressed as:

$$W = W_s + D^2/2\varepsilon \tag{7}$$

where W_s is the strain energy density associated with the in-plane stretches of the material, and $D^2/2\varepsilon$ term is the Helmholtz free energy density associated with electric polarization and the permitivity of the elastomer $\varepsilon = \varepsilon_0 \varepsilon_r$ is a constant independent of deformation. Note that the condition of incompressibility is implied throughout the analyses [15].

Choosing a correct strain energy function, W_s, is the basic process for modeling the electromechanical behaviours of DEA [56]. In order to find the best one, we compare different strain energy functions.

Elastic material model

Over the decades, various strain energy functions have been created. Commonly used strain energy functions include neo-Hookean model, Ogden model and Gent model.

The neo-Hookean model has the advantage of predicting the stress-strain behavior of hyperelastic materials undergoing large deformation. However at large strains, it is not accurately practical [20, 58]. The free energy density of an incompressible neo-Hookean hyperelastic material is given by:

$$W_s = -\frac{\mu_0}{2}(\lambda_x^2 + \lambda_y^2 + \lambda_x^{-2}\lambda_y^{-2} - 3)$$

where μ_0 is the strain shear modulus which is constant; λ_x and λ_y are the pre-stretches of length and width, respectively.

Ogden model, [59], is also one of the popular hyperelastic material models, which can be used to describe the non-linear stress-strain behaviour of materials like polymers, which expresses as:

$$W_s = \sum_{i=1}^{N} -\frac{\mu_{i\lim}}{\alpha_i}\log(\lambda_x^{\alpha_i} + \lambda_y^{\alpha_i} + \lambda_x^{-\alpha_i}\lambda_y^{-\alpha_i} - 3)$$

where N is the number of model order, and μ_i and α_i are the parameters of the material, which can be verified by experiments.

Among these models, the Gent model, [60], is a commonly used energy function for DEs that consist of long and flexible polymer chains. In contrast to Ogden model, Gent model has phisical desccription for the material, which makes it physical based. Also this model accurately predicts the strain-stiffening effect unlike the neo-Hookean model. The Gent model for isotropic incompressible elastomers is fairly straightforward. To account for the stretching limit, the Gent model assumes that:

$$W_s = -\frac{\mu_0 J_{\lim}}{2}\log(1 - \frac{\lambda_x^2 + \lambda_y^2 + \lambda_x^{-2}\lambda_y^{-2} - 3}{J_{\lim}}) \tag{8}$$

where μ_0 is shear modulus, and $J_{\lim}$ is a dimensionless parameter representing the extension limit of the polymer chains. Huang and Suo, [61], used this description to create a schematic for the electromechanical phase transition in an ideal DE membrane, predicting that a certain crucial transition point would occur.

Viscoelasticity of DEs

Material models alone are insufficient to accurately describe the DE's strain behaviour [62]. DEs have nonlinear material properties, which undergo time-dependent dissipative processes, due to the viscoelastic behaviours of the materials. It mainly happens when a dielectric elastomer undergoing voltages over a characteristic time [27, 56]. Viscoelasticity can adversely impact on the dynamic response of DEAs, which would limit their use [63]. In order to accurately model the dynamic behaviour of DEAs, material viscoelasticity has to be considered.

During the last decades, various models have been developed to reflect the material viscoelasticity of DEs such as rheological model, also called Maxwell model, [64] and generalized Kelvin model [65].

One of the most popular method that researchers have used is rheological model which is shown in Figure 7. Rheological model consists of springs and dashpots with many parallel units has been used to examine viscoelastic dielectrics theoretically; the elastic springs are in series with viscous dashpots. The first unit contains an elastic spring, whereas the remaining units contain elastic springs as well as viscoelastic units. The basic rheological elements, springs and dashpot components, can be connected in series or parallel to describe elastic springs [66]. Hong, [67], created a model capable of adopting most hyperelastic constitutive models for viscoelastic solids. This approach provides a convenient way to construct the constitutive relations of viscoelastic DEs.

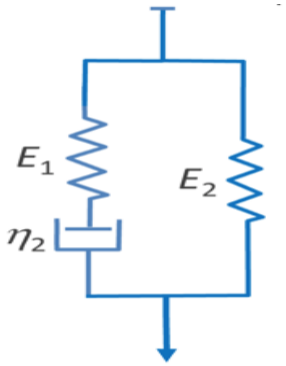

Figure 7: Generalized Maxwell model

The generalized Kelvin model, (see Figure 8), have flexible mechanisms, which makes it popular. This model consists of two parts, which part one is composed of elements including a spring and the other part composed of the springs and dampers in the parallel. In [48], generalized Kelvin model has been used to describe the viscoelastic characteristics of DEA, in order to establish a dynamic model based on thermodynamic theory.

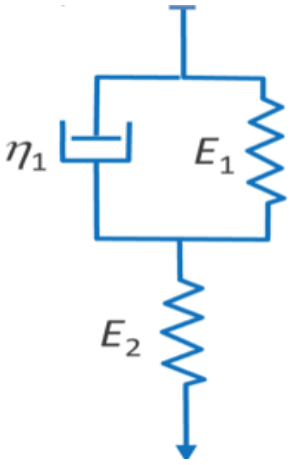

Figure 8: Generalized Kelvin model

Chapter 3

Dynamic modeling of conical DEA

Based on the literature, there are many different methods to describe the complex nonlinear behavior of dielectric elastomer. However, most of the previous studies ignored the complex configuration and used rheological models to describe the nonlinear viscoelasticity. Therefore, the dynamic analysis of DEA with conical geometry based is still a great challenge, which needs to develop.

This section presents a dynamic model of DEA made of PDMS with conical shape to relate the input voltage to the displacement. The model is based on physical phenomena, in which we use thermodynamic nonequilibrium in order to describe the complex nonlinear motion. Also, in this study we choose Gent model and the generalized Kelvin model to describe the elastic energy and the viscoelasticity, respectively.

However, when the geometry is complicated like conical configuration, the nonlinear characteristics such as inhomogenous stress-starin, time-dependent viscoelasticity, and electromechanical coupling become difficult to model [68]. For this reason, the following assumptions are recommended to reduce the model's complexity:

- The radial strain is homogenous along the radial axis.
- The membrane and electrode mass is low in comparison to the biasing weight mass.

3.1 Model description

Figure 9 shows the three states of the DEA; The first state is called undeformed state, the second state is called prestretched state, and the third state is called deformed state [2].

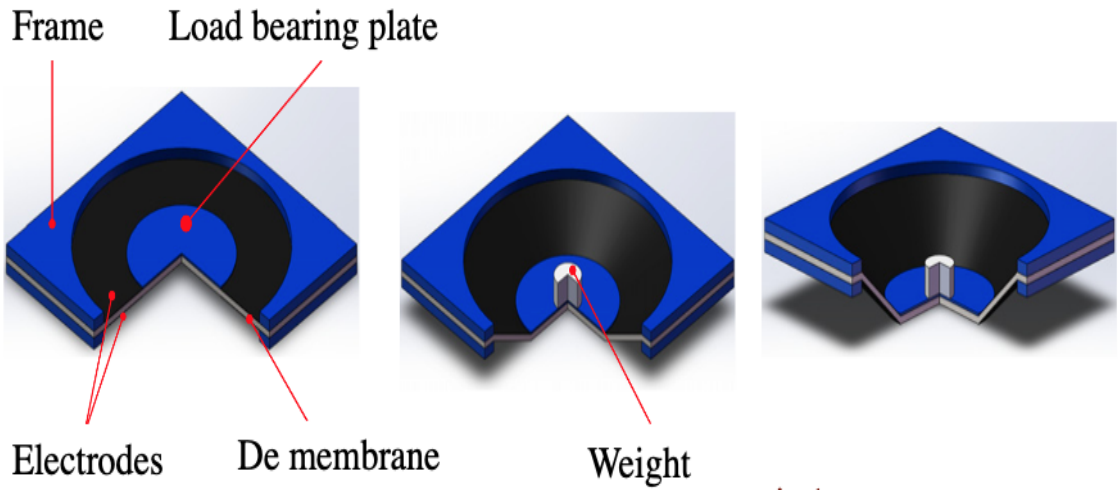

Figure 9: (a) Undeformed state of DEA. (b)prestretched DEA. (c)Deformed state of DEA.

in Figure 10(a), undeformed state, the film with radial length L_0 and thickness h_0 is fixed in a frame of rigid plastic with outer radius b and inner radius a. Then in order to increase the actuator displacement, a weight is put on the center of the frame which objected with the gravity P, that provides a constant loading force.

As shown in Figure 10(b), beacuse of the quasi-static actuation principle, the tension-induced force and the biassing mass force are balanced in the vertical axis, which cause displacement of d_1 in the center to reach the equilibrium point at pre-stretch state. Therefore the conical DEA has prestreatches in radial length, $\lambda_{1,pre}$ and in thickness $\lambda_{3,pre}$. Lead to new dimensions of $L_1 = \lambda_{1,pre} L_0$ and $h_1 = \lambda_{3,pre} h_0$, which are prestretched radial lentgh and thickness, respectively.

When an input voltage ϕ is applied across the DE membrane, Figure 10(c), the electrostatic pressure (Maxwell pressure), induced by the electric field, reduces the

tension on the membrane, which results in a force imbalance. The membrane is then deformed out-of-plane by d_2 until a new equilibrium state is achieved. So we have an expansion in the length, L_2 and a decrease in thickness, h_2, at deformed state. If an AC voltage is applied, the DEA will oscillate around its equilibrium point and the amplitude of this oscillation is a function of the voltage amplitude and frequency.

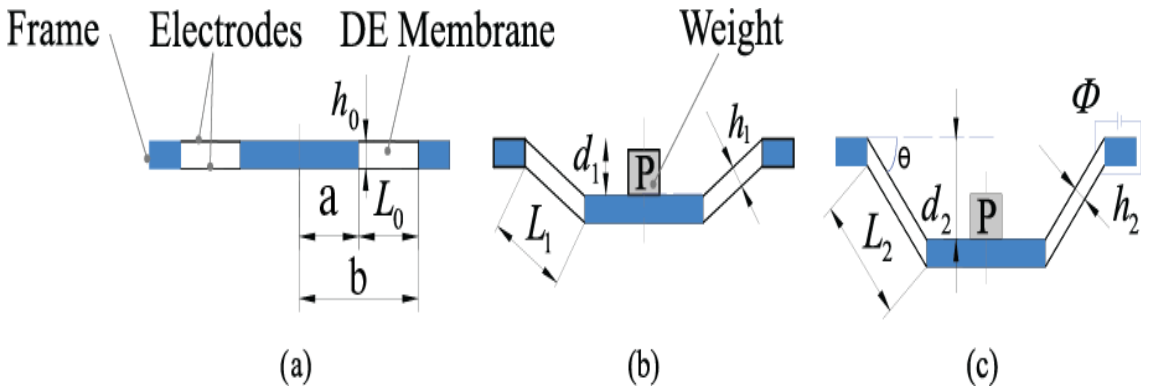

Figure 10: (a) Undeformed state of DEA. (b)prestretched DEA. (c)Deformed state of DEA.

3.2 Model development

As shown in Figure 10, the conical dielectric elastomer, has the initial radial length of $L_0 = b - a$, and the deformed radial length can be obtained by $L_2 = \sqrt{d^2 + (b-a)^2}$. The volume of DEA for undeformed (V_{und}) and deformed (V_{def}) states are:

$$V_{und} = \pi h_0 (b^2 - a^2) \tag{9}$$

$$V_{def} = \pi h_2 L_2 (b + a) \tag{10}$$

Since the DEA is assumed to be homogenous and incompressible [20], the volume, V remains constant during actuation. Therefore we have:

$$V = V_{und} = V_{def} \tag{11}$$

$$\pi h_0 (b^2 - a^2) = \pi h_2 L_2 (b + a) \tag{12}$$

By simplisizing Equation (12) and considering L_0 we obtain:

$$h_0 L_0 = h_2 L_2 \tag{13}$$

So the stretches of the membrane in radial, circumferential and thickness directions, λ_1, λ_2, λ_3, respectively, becomes

$$\lambda_1 = \frac{L_2}{L_0} = \frac{\sqrt{d_2^2 + (b-a)^2}}{(b-a)} \tag{14}$$

$$\lambda_2 = \frac{2\pi}{2\pi} = 1 \tag{15}$$

$$\lambda_3 = \frac{h_2}{h_0} \tag{16}$$

Since the material is incompressible and based on the Equations (9)-(16) we have:

$$\lambda_1 \lambda_2 \lambda_3 = 1, \quad \lambda_1 = \frac{1}{\lambda_3} \tag{17}$$

which agrees with Equation (13). Considering θ as the angle between DE membrane and horizontal direction, as shown in Figure 10(c), by doing some simple algebraic manipulation based on 17 the relationship between λ_1 and d_2 can be expressed as.

$$\sin\theta = \frac{d_2}{L_2} = \frac{\sqrt{\lambda_1^2 - 1}}{\lambda_1} \tag{18}$$

3.3 Dynamic model

To calculate the electromechanical deformation, the princible of nonequilibrium thermodynamics is used. Based on the free energy of DEA and nonequilibrium thermodynamics, the sum of the works done by mechanical force and electric field force is equal or less than the change of the free energy of the DEA. As it shows in Figure 10(c), we only have the mechanical force of P and the vertical displacement of d_2, which is the model's output. As a result, the change of the free energy of the DEA, δG, expresses as:

$$\delta G \leq P \delta d_2 + \phi \delta Q \tag{19}$$

where $P\delta d_2$ is the work done by mechanical force and $\phi\delta Q$ is the work done by electric field. Q is the accumulated charge, which have a relation with the input voltage, ϕ as below

$$Q = \phi C = \phi\frac{\varepsilon\pi l(b+a)}{h_2} = \frac{\varepsilon\phi\pi(b^2-a^2)\lambda_1^2}{h_0} \tag{20}$$

where C and ε is the capacitance and the permittivity of DE material, respectively. From Equations (17) and (20) the charge varies by

$$\delta Q = \frac{\varepsilon\pi(b^2-a^2)}{h_0}(\lambda_1^2\delta\phi + 2\phi\delta\lambda_1) \tag{21}$$

By substituting Equations (9) and (11) in Equation (6), the free energy density for a conical DEA is:

$$W = \frac{G}{\pi h_0(b^2-a^2)}$$

Therefore by substituting Equation (21) into Equation (19) and combing with W we obtain:

$$\delta W \leq \frac{P}{\pi h_0(b^2-a^2)}\delta d_2 + \varepsilon\frac{\phi}{h_0^2}(\lambda_1^2\delta\phi + 2\phi\delta\lambda_1) \tag{22}$$

According to Equations (13)–(18), the relationship between $\delta\lambda_1$ and δd_2 is

$$\delta d_2 = \frac{(b-a)\lambda_1}{\sqrt{\lambda_1^2-1}}\delta\lambda_1 = \frac{(b-a)}{\sin\theta}\delta\lambda_1 \tag{23}$$

Considering (16)-(17), by submitting Equation (23) into Equation (22) we can get

$$\delta W \leq \frac{P}{\pi h_2(b+a)\sin\theta}\frac{\delta\lambda_1}{\lambda_1} + \varepsilon\frac{\phi}{h_0^2}(\lambda_1^2\delta\phi + 2\phi\delta\lambda_1) \tag{24}$$

By deviding L_2 from V_{def} in Equation (9), we can obtain the radial area, $A_{radial} = \pi h_2(b+a)$. Therefore, in Figure 10(c), by balancing forces in the vertical direction, the radial stress of DEA, σ_1 is defined as

$$\sigma_1 = \frac{P}{\pi h_2(b+a)\sin\theta} \tag{25}$$

By substituting Equation (24) in Equation (25) we can get

$$\delta W \leq \frac{\sigma_1}{\lambda_1}\delta\lambda_1 + \varepsilon\frac{\phi}{h_0^2}(\lambda_1^2\delta\phi + 2\phi\delta\lambda_1) \tag{26}$$

In order to solve (26), we need to describe the free energy density and visoelastic behaviour of DEA. Therefore, we have choosen the Gent model and generalized Kelvin

model [48, 65] to describe the free energy density and nonlinear visoelastic behaviour of DEA. As shown in Figure 11, the generalized kelvin model consists of two parts: the part A includes the spring characterized by the Gent model and part B includes series elements which have parallel springs and dashpots to describes the rate-dependent hysteresis in the strain-stress function.

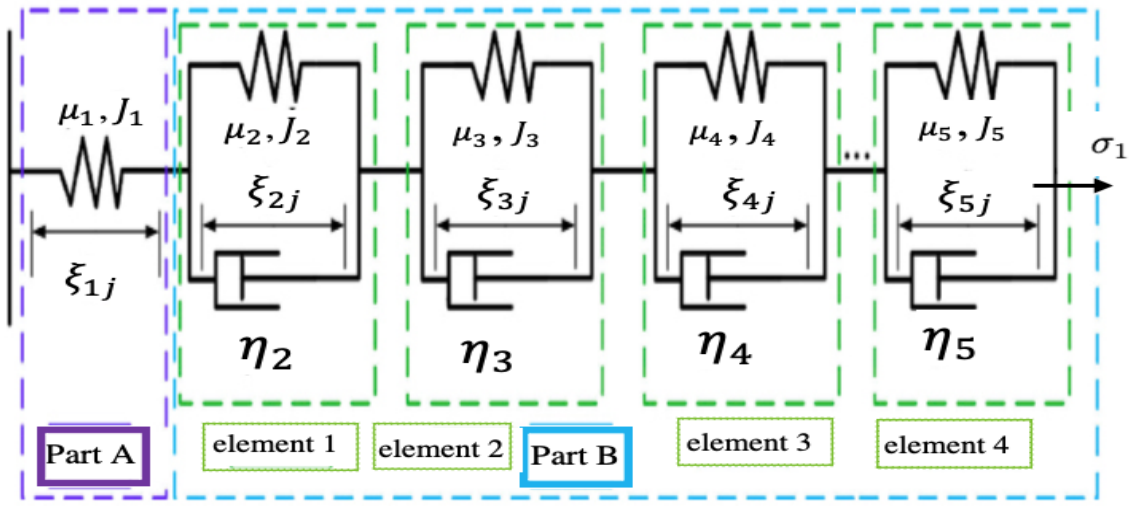

Figure 11: The generalize Kelvin viscoelastic model of the elastomer.

As you can see in figure 7, the dashpot has the same strain as the nonlinesr spring. So ξ_{ij} is the elastic deformation of each element where $(i = 1, 2, 3, ...)$ represents the number of springs in the generalized Kelvin model and $j(= 1, 2)$ defines the vertical direction and horizontal direction, respectively. Since, all elements are in series, DEA's total deformation equals the sum of each element's deformation, that is $\lambda_1 = \sum_{i=1}^{n} \xi_{i1}$, $\lambda_2 = \sum_{i=1}^{n} \xi_{i2}$

Using the generalized Kelvin model to Equation (7), the free energy density of the ideal DEA is function of ξ_{ij} and the electric displacement $D = \varepsilon E$, where $E = \phi/h$ is the electric field.

$$W(D, \xi_{11}, \xi_{12}, \xi_{21}, \xi_{22}, \ldots) = W_s(\xi_{11}, \xi_{12}, \xi_{21}, \xi_{22}, \ldots) + \frac{D^2}{2\varepsilon} \tag{27}$$

ε is the permitivity of the dielectric elastomer and the internal free energy density of DEA W_s can be expressed based on the Gent model [48].

$$W_s = -\sum_{i=1}^{n} \frac{\mu_i J_i}{2} \ln(1 - \frac{\xi_{i1}^2 + \xi_{i2}^{-2} + \xi_{i1}^{-2}\xi_{i2}^{-2} - 3}{J_i}) \tag{28}$$

where μ_i and J_i represent the shear modulus of the ith spring, and the deformation limit of the ith spring, respectively (see Figure 10). ξ_{i1} and ξ_{i2} are the stretches related to each element.

Therefore by combining Equations (27) and (28), we get

$$W = -\sum_{i=1}^{n} \frac{\mu_i J_i}{2} \ln(1 - \frac{\xi_{i1}^2 + \xi_{i2}^{-2} + \xi_{i1}^{-2}\xi_{i2}^{-2} - 3}{J_i}) + \frac{D^2}{2\varepsilon} \tag{29}$$

According to the Newtonian law of mechanics for figure 6, the stress along is the same for each elemnt [69]. Therefore, for element 1, the true stress is σ_1. Combining Equations (26) and (29) the true stress can be expressed as

$$\sigma_1 = \frac{\mu_1(\xi_{11}^2 - \xi_{11}^{-2}\xi_{12}^{-2})}{1 - (\xi_{11}^2 + \xi_{12}^2 + \xi_{i1}^{-2}\xi_{12}^{-2} - 3)/J_1} - \varepsilon(\frac{\phi}{h_2})^2 \tag{30}$$

Considering the viscoelastic coefficient of damper, defined as η_i, where i represent the number of dampers, the mechanical relationship of each element in the generalised Kelvin model can be expressed as:

$$\sigma_1 = \sigma_{i1} + \eta_i \frac{d\xi_{i1}}{dt} \tag{31}$$

where σ_{i1} represent the elastic stress related to ith element in Figure 10. According to Equations (30)-(31), we have

$$\frac{d\xi_{i1}}{dt} = -\frac{1}{\eta_i}(\mu_1 \frac{\xi_{11}^2 + \xi_{11}^{-2}\xi_{12}^{-2}}{1 - (\frac{\xi_{11}^2 + \xi_{12}^2 + \xi_{11}^{-2}\xi_{12}^{-2} - 3}{J_1})} - \mu_i \frac{\xi_{i1}^2 + \xi_{i1}^{-2}\xi_{i2}^{-2}}{1 - (\frac{\xi_{i1}^2 + \xi_{i2}^2 + \xi_{i1}^{-2}\xi_{i2}^{-2} - 3}{J_i})}) \tag{32}$$

where $(i = 1, 2, 3, ...)$ represents the number of springs in the generalized Kelvin model. When $\phi = 0$, we just have the prestretching stress, so $\lambda_1 = \lambda_{1p}$, $\lambda_2 = 1$, then $\xi_{i1} = \lambda_{1p}$, $\xi_{i2} = 1$, substituting into these parameters into Equation (30), we can obtain

$$\sigma_1 = \mu_1(\frac{\lambda_{1p}^2 - \lambda_{1p}^{-2}}{1 - (\lambda_{1p}^2 + \lambda_{1p}^{-2} - 2)/J_1}) \tag{33}$$

When $\phi = 0$, we have $\lambda_1 = \lambda_{1p}$, and based on (18), $\sin\theta = \frac{\sqrt{\lambda_{1p}^2 + (b-a)^2}}{\lambda_{1p}}$ and $h_2 = h_0$. Therefore, by substituting Equation (33) into Equation (25), When $\phi = 0$, P can be calculated as

$$P = \pi h_0(a+b)\frac{\sqrt{\lambda_{1p}^2 - 1}}{\lambda_{1p}^2}\mu_1(\frac{\lambda_{1p}^2 - \lambda_{1p}^{-2}}{1 - (\lambda_{1p}^2 + \lambda_{1p}^{-2} - 2)/J_1}) \tag{34}$$

Also, we can find the relation between P and ϕ, by substituting Equation (25) in equation (30), which can be presented as

$$P = \pi h_0(a+b)\frac{\sqrt{\lambda_1^2-1}}{\lambda_1^2}\mu_1\left(\frac{\xi_{11}^2 - \xi_{11}^{-2}\xi_{12}{}^{-2}}{1-({\xi_{11}}^2+{\xi_{12}}^2-{\xi_{11}}^{-2}{\xi_{12}}^{-2}-3)/J_1} - \frac{\varepsilon\phi^2}{h_2^2}\right) \tag{35}$$

Since, all elements are in series, DEA's total deformation is $\lambda_1 = \sum_{i=1}^{n}\xi_{i1}$. So we can rewrite equation (35) as

$$P = \pi h_0(a+b)\frac{\sqrt{(\sum_{i=1}^{n}\xi_{i1})^2-1}}{(\sum_{i=1}^{n}\xi_{i1})^2}\mu_1\left(\frac{{\xi_{11}}^2 - {\xi_{11}}^{-2}{\xi_{12}}^{-2}}{1-\frac{({\xi_{11}}^2+{\xi_{12}}^2-{\xi_{11}}^{-2}{\xi_{12}}^{-2}-3)}{J_1}} - \frac{\varepsilon\phi^2(\sum_{i=1}^{n}\xi_{i1})^2}{h_0^2}\right) \tag{36}$$

Taking derivative of both sides of Equation (36) with respect to time, we can get

$$\frac{dP}{dt} = \frac{\partial P}{\partial \phi}\frac{d\phi}{dt} + \sum_{i=1}^{n}\frac{\partial P}{\partial \xi_{i1}}\frac{d\xi_{i1}}{dt} + \sum_{i=1}^{n}\frac{\partial P}{\partial \xi_{i2}}\frac{d\xi_{i2}}{dt} \tag{37}$$

Since P given by (32) is constant, then $\frac{dP}{dt} = 0$. Also there is no change in the horizontal stretch of DEA respect to time, then $\frac{d\xi_{i2}}{dt} = 0$. Thus, Equation (37) can be rewritten as

$$\frac{d\xi_{11}}{dt} = -\left(\frac{\partial P}{\partial \phi}\frac{d\phi}{dt} + \sum_{i=1}^{n}\frac{\partial P}{\partial \xi_{i1}}\frac{d\xi_{i1}}{dt}\right)/\frac{\partial P}{\partial \xi_{11}} \tag{38}$$

3.4 Model summary

Combining Equations (32), (38), and considering the fact we just have the vertical force and displacement, the dynamic model of the conical DEA can be described as

$$\begin{gathered}
\frac{d\xi_{11}}{dt} = -\left(\frac{\partial P}{\partial \phi}\frac{d\phi}{dt} + \sum_{i=1}^{n}\frac{\partial P}{\partial \xi_{i1}}\frac{d\xi_{i1}}{dt}\right)/\frac{\partial P}{\partial \xi_{11}} \\
\frac{d\xi_{12}}{dt} = 0 \\
\frac{d\xi_{i1}}{dt} = -\frac{1}{\eta_i}\left(\mu_1\frac{\xi_{11}^2+\xi_{11}^{-2}}{1-(\frac{\xi_{11}^2+\xi_{11}^{-2}-2}{J_1})} - \frac{\mu_i}{\eta_i}\frac{\xi_{i1}^2+\xi_{i1}^{-2}}{1-(\frac{\xi_{i1}^2+\xi_{i1}^{-2}-2}{J_i})}\right) \\
\frac{d\xi_{i2}}{dt} = 0
\end{gathered} \tag{39}$$

This model represents the dynamics of the conical DEA and builds the relationship between the input voltage and the displacement of the actuator. In the next section the model parameters are determined by fitting the data to the experimental results using a differential evolution algorithm in MATLAB.

Chapter 4

Experimental set up and model validation

4.1 Experimental set up

In this section, the process for fabrication of the conical DEA is briefly illustrated.Then the experimental model validation is discussed. The dynamic model's correctness is illustrated by comparing the modelled and experimental results.

4.1.1 Fabrication and experimental characterization

Figure 12 shows the five components to fabricate the conical DEA which includes:

- DE membrane which is made of Polydimethylsiloxane msterial (PDMS); Wacker Chemie AG, Germany; Undeformed thickness: $h_0 = 200\mu m$.
- Frame with Polymethyl methacrylate material (PMMA) and inner circle radius of $R = 6cm$.
- Load-bearing plate (Material: PMMA; Radius: R0 = 3cm)
- Electrode (Material number: DD-10; Manufacturer: Saidi Technology, China).
- Weight

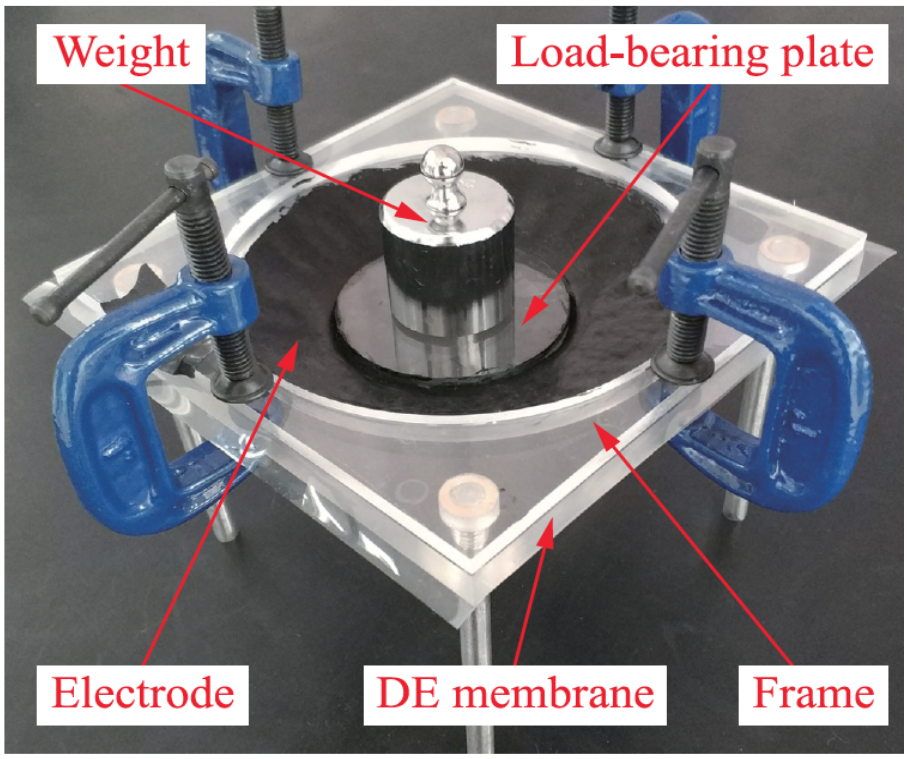

Figure 12: Structure of conical DEA (adopted from [2]).

To eliminate the wrinkle of the DE film, we repeatedly adjusted the pose of the load-bearing plate. Meanwhile, the DEA was left standing for a long period before each trial to allow the wrinkle to disappear gradually. The DE film has less wrinkles in the experiment as a result of the foregoing methods; the effect of wrinkling on electrical deformation is minimised; and the validity of experimental data is ensured.

4.1.2 Experimental method

The detailed experimental setup is described as follows (see Figure 13).

- A high voltage amplifier (Model number: 10/40A-HS-H-CE; Manufacturer: TREK, USA) on the DEA during deformation to amplify the original voltage signal by 1000 times and apply it to the electrodes of the DEA.
- A laser distance sensor (Model number: LK-H152; Manufacturer: Keyence, Japan) to detect the displacement measurements of membrane undergoing high voltage power.

- I/O module (Model number: PCIe-6361; Manufacturer: National Instruments, USA) to record real-time displacement data from the laser sensor and output an original voltage signal for the high voltage amplifier.
- The DEA (Material: Polydimethylsiloxane (PDMS)) to do the experimental test on it.
- Finally a Computer (CPU: i7-8700; Memory: 16G; Manufacturer: Hewlett Packard, USA) to analyze the data.

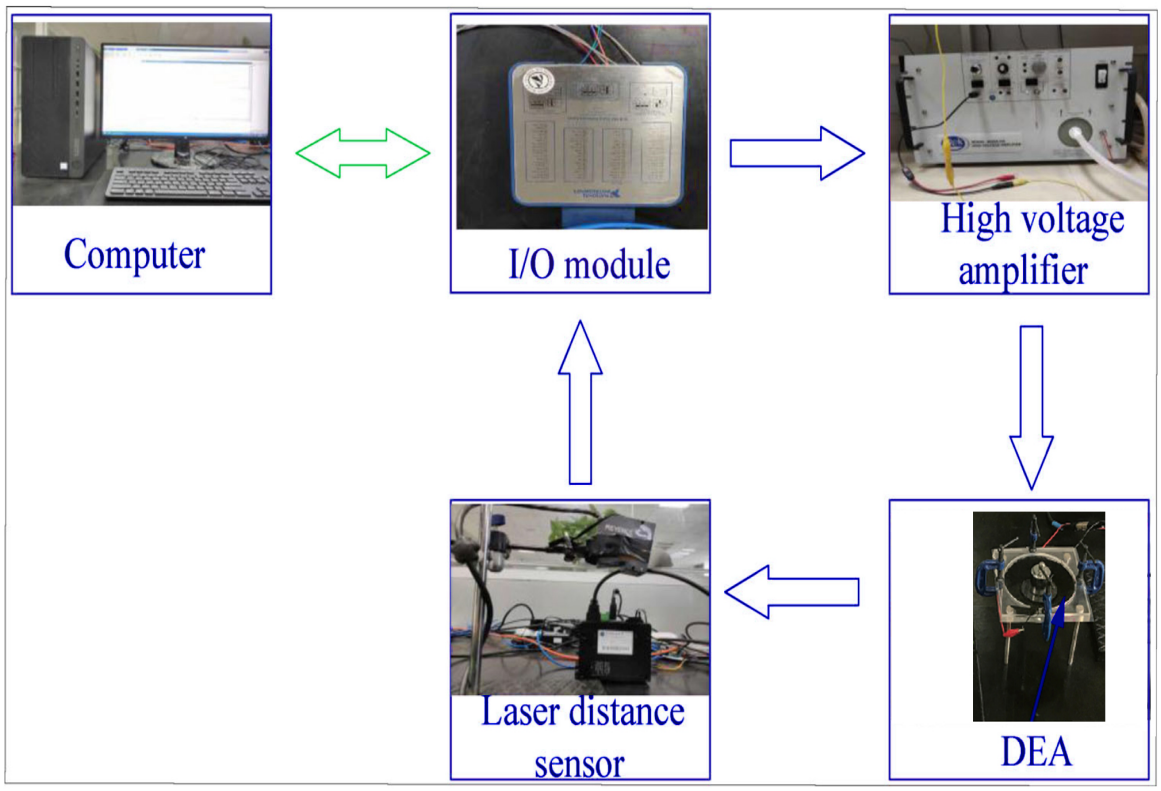

Figure 13: Block diagram of experimental platform, which includes five components: computer, high voltage amplifier, laser distance sensor, I/O module and conical DEA.

4.2 Parameter identification and validation

In this section, experiments were conducted to verify the analytical model. First, the undetermined parameters are identified based on the differential evolution algorithm using MATLAB/Simulink to implement the algorithms with various patterns of voltage and frequencies. Next, the model simulations are tested and compared with the experimental results.

Driving voltage

Based on the real experiments, the dynamic behavior of the DE was actuated under different driving voltages.

$$
\begin{cases}
t_m = rem\left(t, \sum_{i=1}^{5} 1/f_i\right) & \\
v(t_m) = a_1 \sin\left(f_1 \pi t_m\right), & 0 \leqslant t_m \leqslant 1/f_1 \\
v(t_m) = a_2 \sin\left(f_2 \pi t_m - f_2 \pi / f_1\right), & 1/f_1 \leqslant t_m \leqslant \sum_{i=1}^{2} 1/f_i \\
v(t_m) = a_3 \sin\left(f_3 \pi t_m - f_3 \pi \sum_{i=1}^{2} 1/f_i\right), & \sum_{i=1}^{2} 1/f_i \leqslant t_m \leqslant \sum_{i=1}^{3} 1/f_i \\
v(t_m) = a_4 \sin\left(f_4 \pi t_m - f_4 \pi \sum_{i=1}^{3} 1/f_i\right), & \sum_{i=1}^{3} 1/f_i \leqslant t_m \leqslant \sum_{i=1}^{4} 1/f_i \\
v(t_m) = a_5 \sin\left(f_5 \pi t_m - f_5 \pi \sum_{i=1}^{4} 1/f_i\right), & \sum_{i=1}^{4} 1/f_i \leqslant t_m \leqslant \sum_{i=1}^{5} 1/f_i
\end{cases}
$$

where a_i and f_i, (i = 1, 2, . . ., 5), are the amplitudes and the frequencies, respectively. $t \in [0, +\infty)$ is time and $rem(m, n)$ is the remainder of m divided by n, in which $t_m = rem(t, \sum_{i=1}^{5} 1/f_i)$. Therefore, by changing the values of a_i and f_i, a periodic driving voltage with different frequency and amplitude is generated.

The amplitudes of the driving voltages are chosen to be $a_i = 5.5 + 0.5i(kV)$ and the frequencies are chosen to be $f_i = 0.2i(Hz)$. Figure 14 shows, the diagram of driving voltage, where the period is $T = \sum_{i=1}^{5} 1/f_i$.

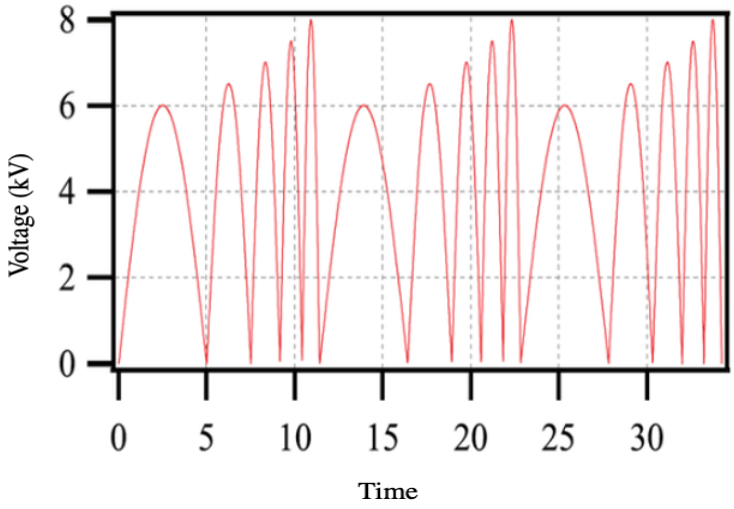

Figure 14: The driving voltage used in parameter identification

Model identification

In this part, the parameters of the dynamic model in (39) are identified based on the experimental results, using the differential evolutionary algorithm. Differential evolution is a method for solving nonlinear and multidimensional problems by finding approximate solutions, optimising real parameters, and evaluating real-valued functions.

In this model we do not have any prior knowledge about the values of $J_i, \mu_i$and η_i, so we use the differential evolutionary algorithm to identify the optimal solution. The parameter identification process by using the differential evolutionary algorithm is shown in Algorithm 1.

Algorithm 1 differential evolutionary algorithm

Input : Input voltage signal, material and geometrical parameters.

Output: Predictions of time-dependet electromechanical response of the actuator

1: ***begin***
2: Input the dielectric permitivity ε of the material.
3: Input the geometrical parameters, L_0, L_1, h_0, d_1 in Table (1)
4: Input the voltage signal in Figure (14),
5: Define the serache ranges of variable μ_i, j_i and η_i as Ω_1, Ω_2 and Ω_3, respectively. Then, initialize g=0.
6: According to Ω_1, Ω_2 and Ω_3, randomely initialize the initial population as $x_k(0)(k = 1, 2, ..., N)$, where $x_k(0) = \{\tilde{\mu}_i^k(0), \tilde{j}_i^k(0), \tilde{\eta}_i^k(0)\}$
7: **for** $g = 0 : G$ **do**
8: substituting $x_k(g)$ into (39). Then, call ode15s solver to get $\tilde{\xi}_{i1}^k(g)$ and $\tilde{\xi}_{i2}^k(g)$ by solving (39).
9: According to the experimental data and $\tilde{\xi}_{i1}^k(g)$, $\tilde{\xi}_{i2}^k(g)$, calculate error.
10: **if** $e_{rms} \leq \delta$ **then** (δ is a small positive constant),
11: The parameters in dynamic model (39) are obtained. That is $\mu_i = \tilde{\mu}_i^k(0)$, $j_i = \tilde{j}_i^k(0)$ and $\eta_i = \tilde{\eta}_i^k(0)$
12: **end if**
13: According to the mutation rate p_{mr} and the crossover rate p_{cr}, update $x_k(g)$ by executing mutation operation, crossover operation and selection operation in turn.
14: **end for**=0

As a part of the initialization step, the search ranges of the values (maximum and minimum) of the required parameters should be defined. Therefore the search ranges of μ_i, j_i and η_i are set as $\Omega_1 \in (10^2, 6 \times 10^8)$, $\Omega_2 \in (10^0, 8 \times 10^6)$ and $\Omega_3 \in (10^2, 9 \times 10^7)$, respectively. The population size is 240 and the maximum number of evolution is set to be $G = 115$. The constant, δ is set as 0.001. The mutation rate p_{mr} and crossover rate p_{cr} are set to be 0.6 and 0.9, respectively. Moreover, the permittivity of DEA is $\epsilon = 4.7\epsilon_{air}$, where $\epsilon_{air} = 8.85 \times 10^{-2}$ is the permittivity of vacuum. The geometrical parameters, which are used in differential evolution algorithm are listed in the Table 1.

Initial parameters	Value
b	0.03 (m)
a	0.06 (m)
L_0	0.03 (m)
h_0	0.0002 (m)
L_1	0.0325 (m)
h_1	0.000216 (m)
d_1	0.01256 (m)
λ_0	1.084
x_0	(1.084, 0, 1.084, 0.922, 1.084, 0.922, 1.084, 0.922, 1.084, 0.922)
m	0.21 (kg)
P	2.058 (N)

Table 1: Definition of the different parameters used to describe the geometry and mechanical properties of the frame and the membrane.

In order to obtain the accuracy of the presented model in (39), the root-mean-square error of the modelling and the maximum modelling error are defined as below:

$$e_{rms} = \sqrt{\frac{1}{N_p}\sum_{i=1}^{N_p}(D_{Ei} - D_{Mi})^2} \times 100\%$$

$$e_m = \frac{Max(|D_{Ei} - D_{Mi}|)}{Max(D_{Mi}) - Min(D_{Mi})} \times 100\%$$

where D_{Ei} and D_{Mi} represent the experimental data and the model predicted value of the displacement in the vertical direction. Figure 15, shows the error between the model prediction and the experimental result $D_{Ei} - D_{Mi}$.

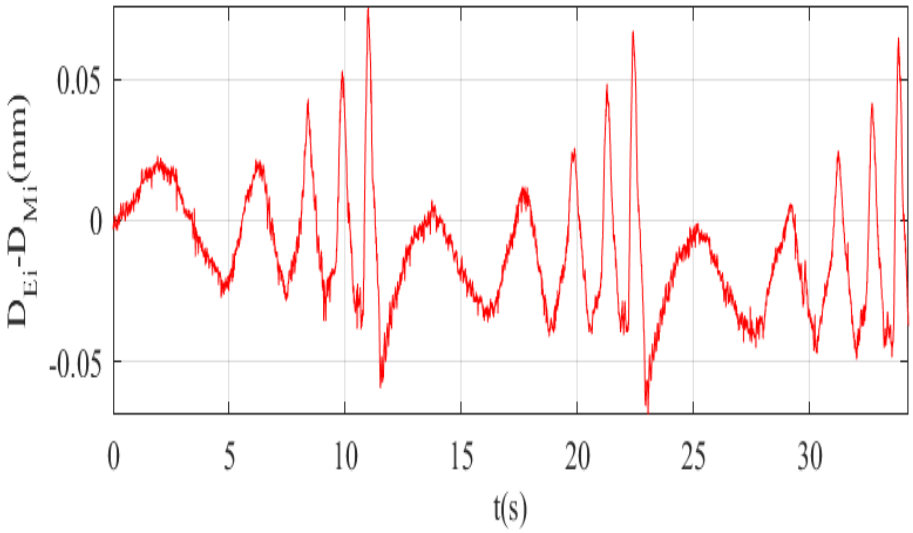

Figure 15: Error between model prediction and experimental result.

i	μ_i	j_i	η_i
1	3.149×10^5	3.109×10^4	no dashpot
2	5.552×10^6	1.016×10^6	555.205
3	5.232×10^8	7.817×10^6	5.232×10^4
4	100	7.927×10^6	8.103×10^7
5	1.573×10^5	2	1.573×10^5

Table 2: Parameter identification results of conical DEA.

The root-mean-square error e_{rms} is 2.42% and the maximum tracking error e_m is 4.53%. Therefore, using the differential evolution algorithm in MATLAB (SIMULINK), we identify the dynamic model parameters as presented in the Table 2. Figure 16 show the comparison of model prediction and experimental result with different driving voltage amplitudes and different frequencies.

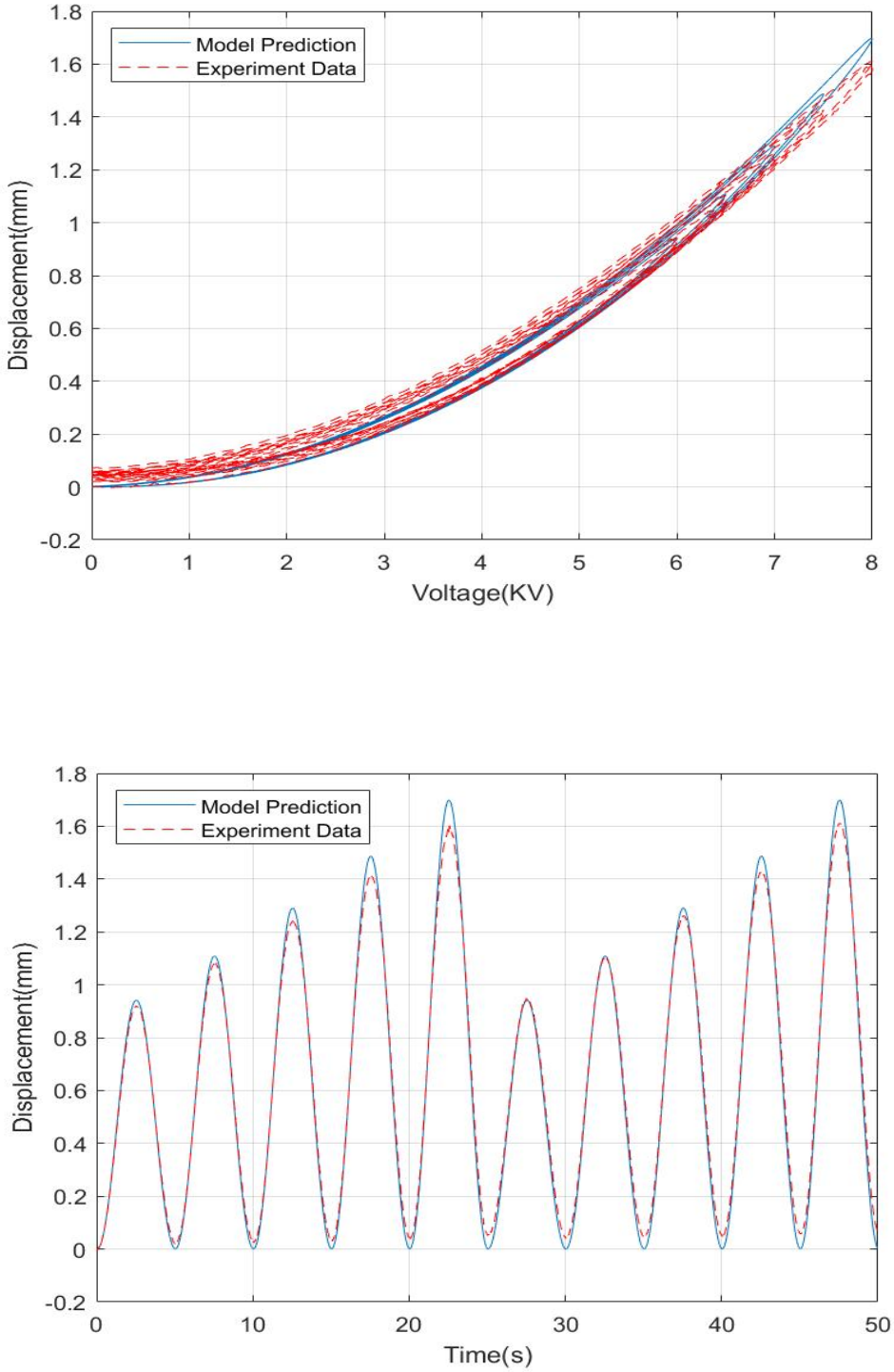

Figure 16: Comparison of model output and experimental result with different amplitudes and frequencies.

4.3 Model validation

In this section, the generalization of dynamic model (39) is verified by setting different values of a_i and f_i. The validation includes two sets of experiments. First, the model is verified with different driving voltage frequencies. Then, the model is verified with different driving voltage amplitude

4.3.1 Model validation with different voltage frequencies

In the first set of experiments, the amplitudes of the driving voltage are set to $a_i = 6.0, 6.5, 7.0, 7.5, 8.0(kV)$, respectively. Meanwhile, the frequencies are set to be $f_i = 0.2(Hz)$, where (i = 1, 2, ..., 5). Thus, the driving voltage has various frequencies but single amplitude in each test experiment. Figures 17 to 21 show the comparisons of the model prediction and the experimental data with different driving voltage frequencies. The modeling error for all test experiments with different driving voltage frequencies are shown in Table 3.

i	f_i	e_{rms}	e_r
1	0.2	3.66	7.41
2	0.4	4.03	6.74
3	0.6	4.18	7.11
4	0.8	3.82	6.38
5	1	3.50	5.86

Table 3: Modeling errors with different driving voltage frequencies.

According to the above results, the root mean-square error of the modeling for test experiments with different driving voltage frequencies is less than 4.18%. The maximum modeling error for any test experiment is less than 7.41%. For higher frequencies, the maximum modelling error is reduced except for the frequency of 0.2Hz. The reason for this is because when the driving voltage frequency is higher, external disturbances have less of an impact on data collecting. Although the maximum modeling error is high, it is still within the allowable range. Therefore, the validation of the proposed dynamic model is verified.

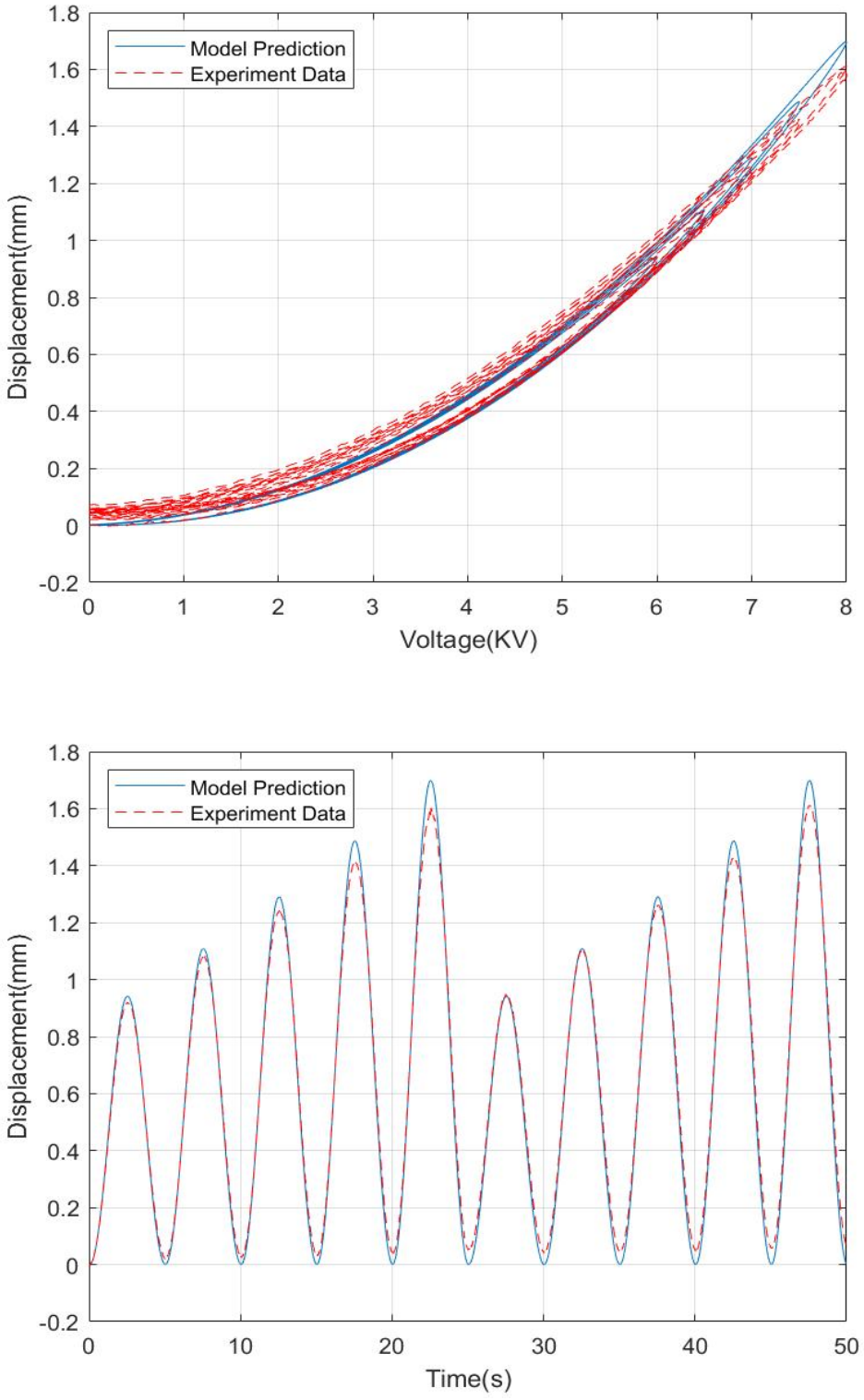

Figure 17: Comparison of model output and experimental result with driving voltage frequency 0.2Hz.

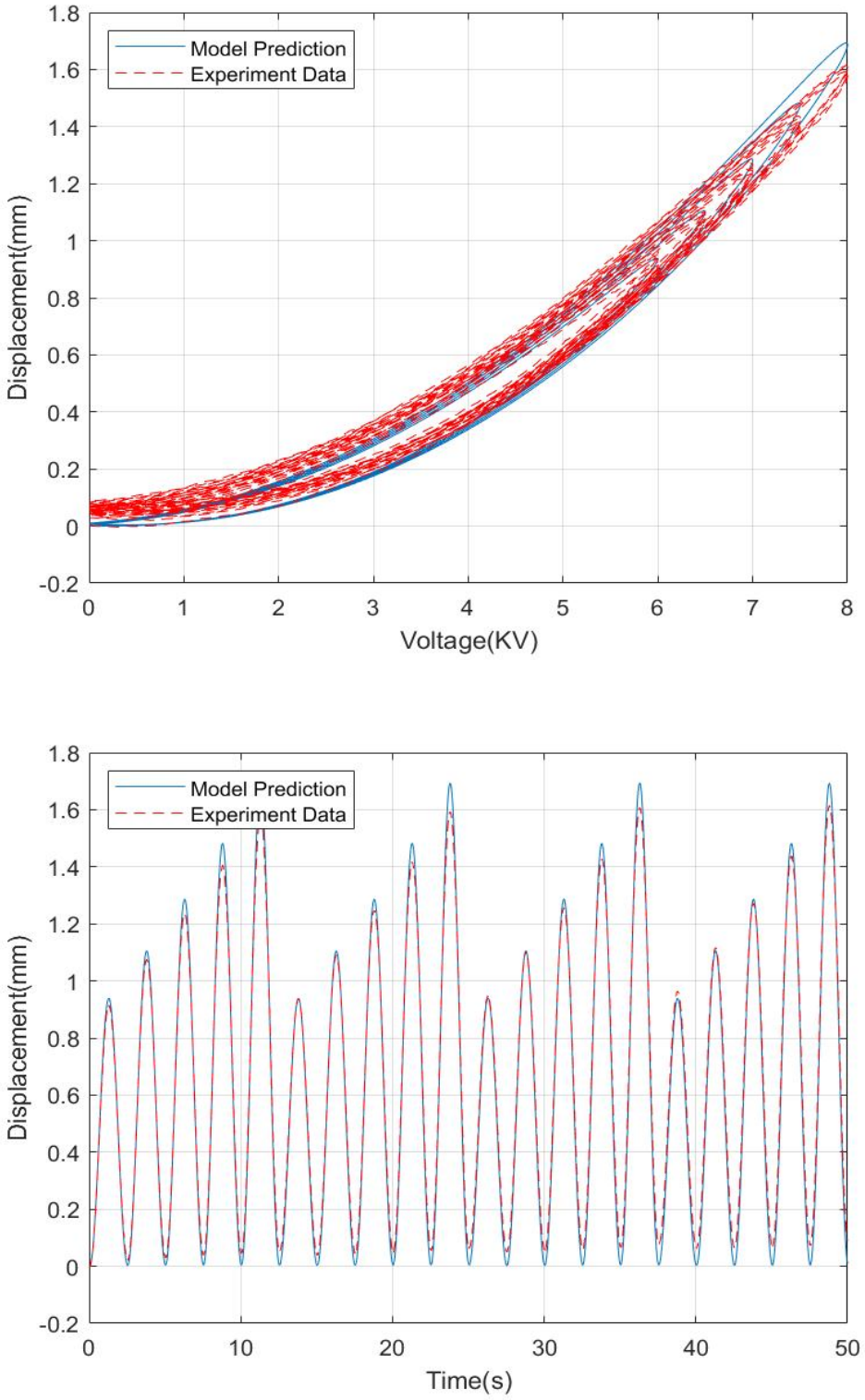

Figure 18: Comparison of model output and experimental result with driving voltage frequency 0.4Hz.

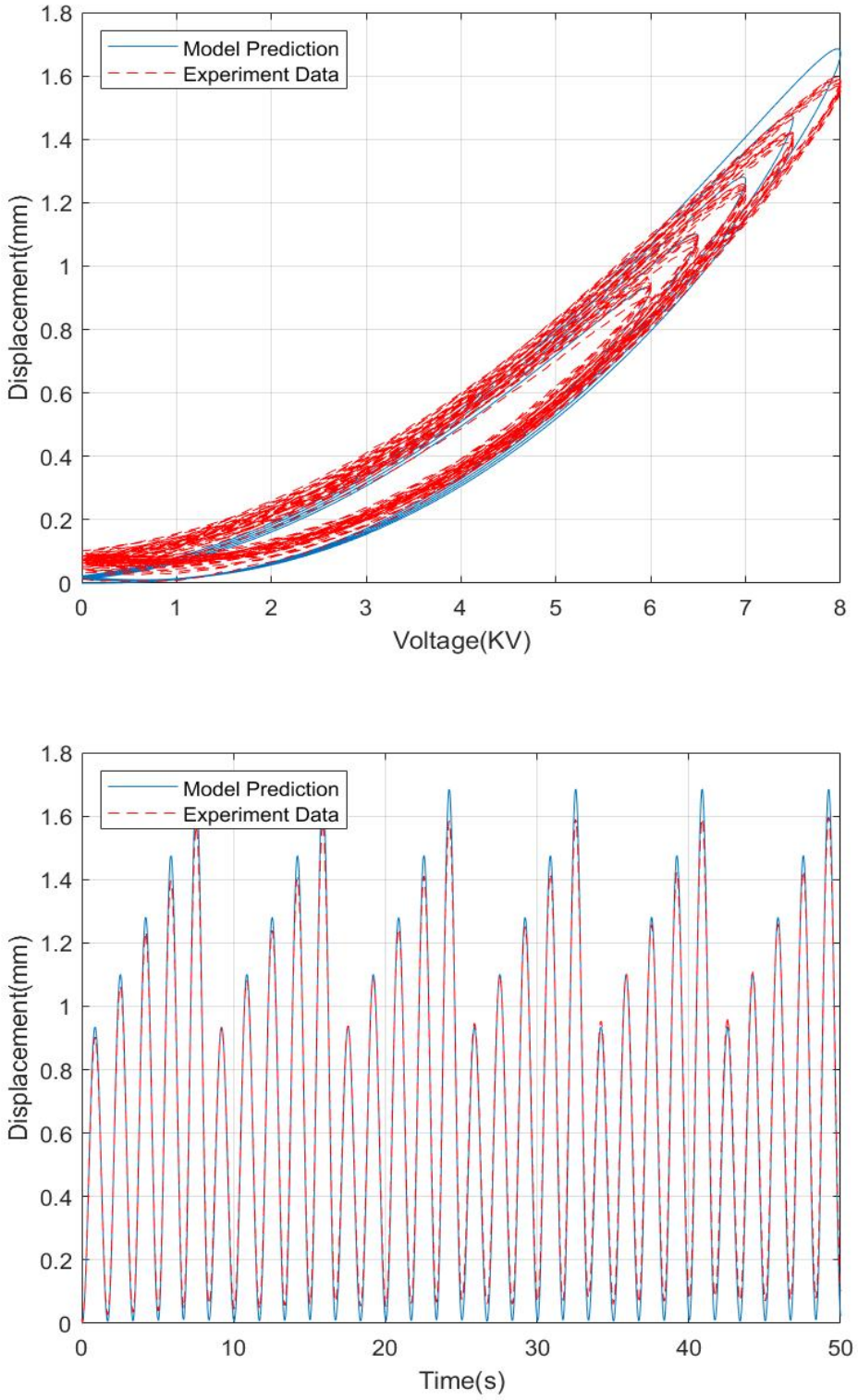

Figure 19: Comparison of model output and experimental result with driving voltage frequency 0.6Hz.

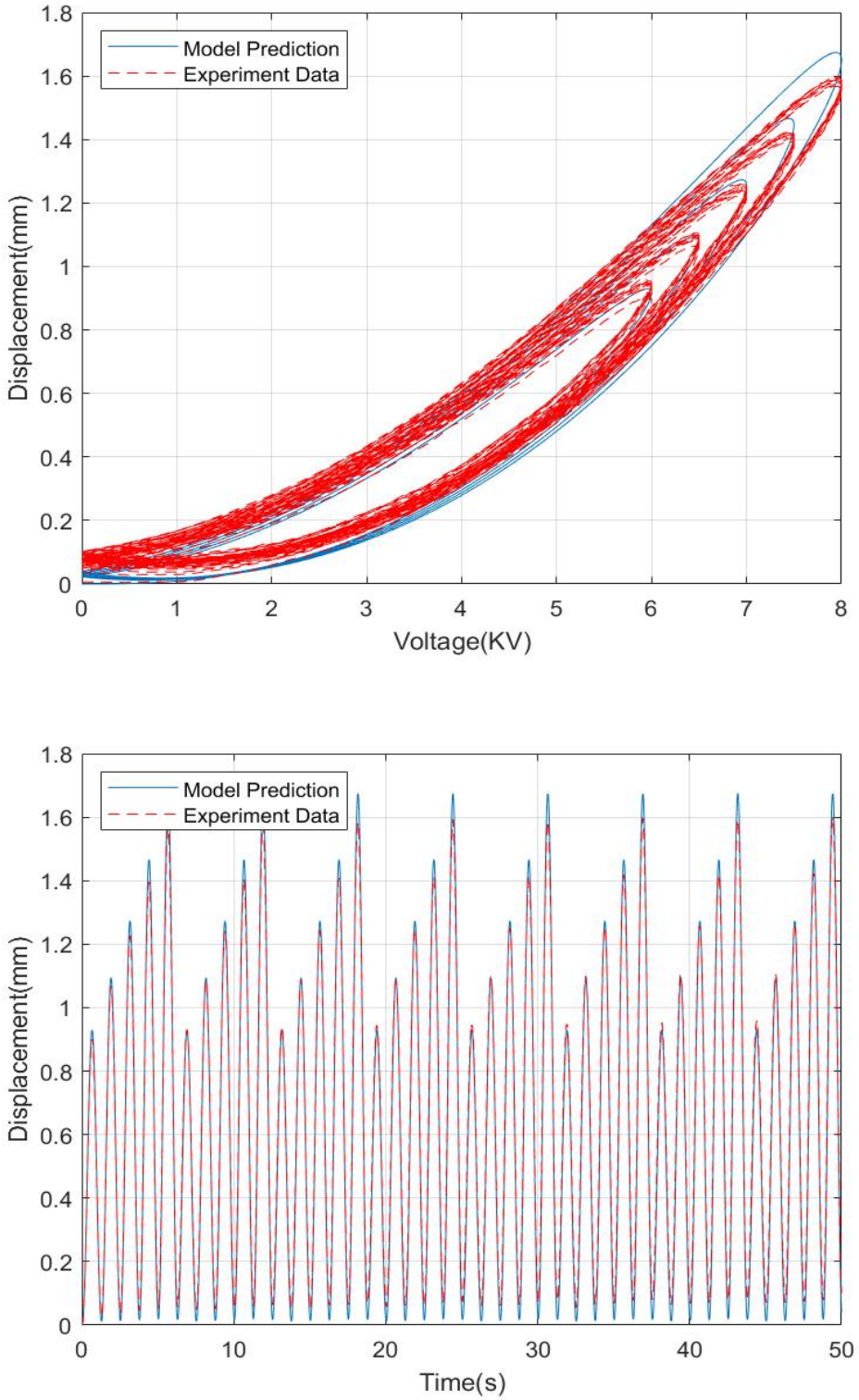

Figure 20: Comparison of model output and experimental result with driving voltage frequency 0.8Hz.

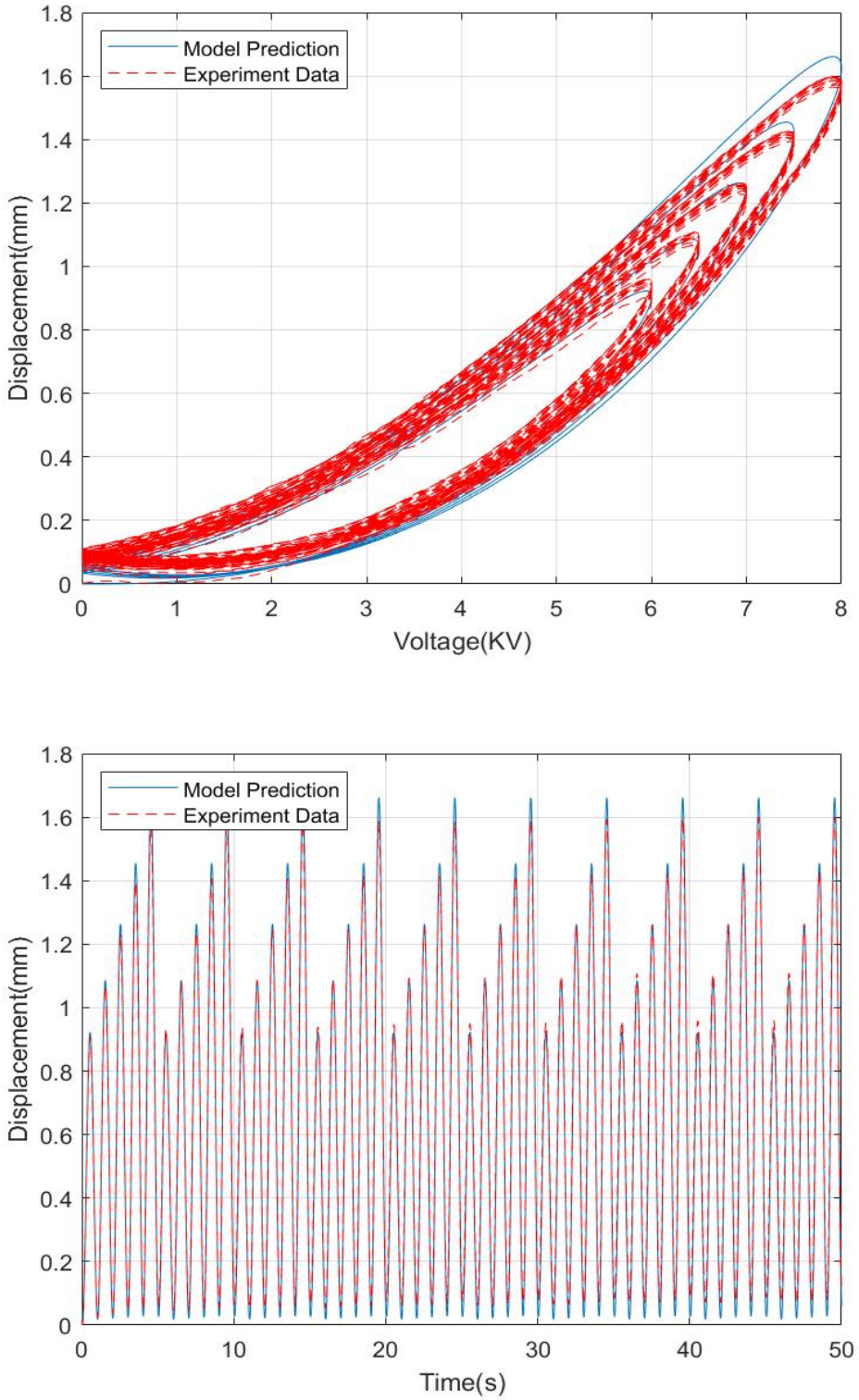

Figure 21: Comparison of model output and experimental result with driving voltage frequency 1Hz.

4.3.2 Model validation with different voltage amplitudes

In the second set of experiments, the amplitudes of the driving voltage are set to be $a_i = 5.5 + 0.5i(kV)$, where (i = 1, 2, . . ., 5). Moreover, $f_i = 0.2, 0.4, 0.6, 0.8, 1(Hz)$, respectively. So, the driving voltage has various amplitudes but single frequency in each test experiment. Figures 22 to 26 shows the comparisons of the model prediction and the experimental data with different driving voltage amplitudess. The modeling errors for all test experiments with different driving voltage amplitudes are shown in Table 4.

i	a_i	e_{rms}	e_r
1	6	1.91	1.93
2	6.5	1.81	3.22
3	7	2.53	3.84
4	7.5	3.74	4.07
5	8	5.03	5.45

Table 4: Modeling errors with different driving voltage amplitudes.

According to the above results, by increasing the amplitude of driving voltage, both the root mean-square error and the modeling error are increased. Where the maximum root mean-square error and the maximum modeling error is for $a_i = 8$, which are 5.03% and 5.45% respectively. Despite the fact that the maximum modelling error is large, it is still within the acceptable range. As a result, the proposed model's generalisation is acceptable.

In the above works, we verify the model driving by the voltage with different amplitudes and frequencies, respectively.

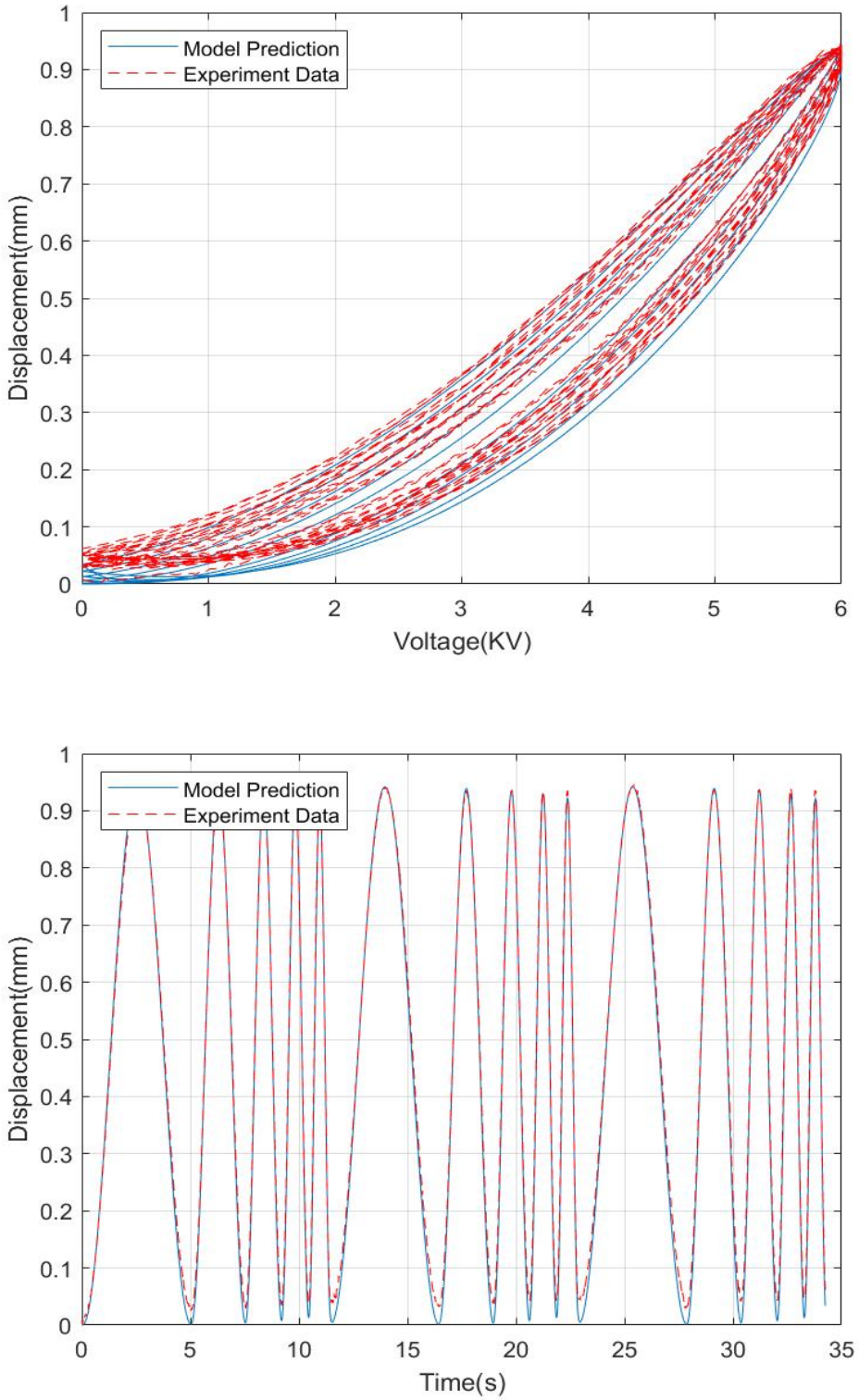

Figure 22: Comparison of model output and experimental result with driving voltage amplitude 6kv.

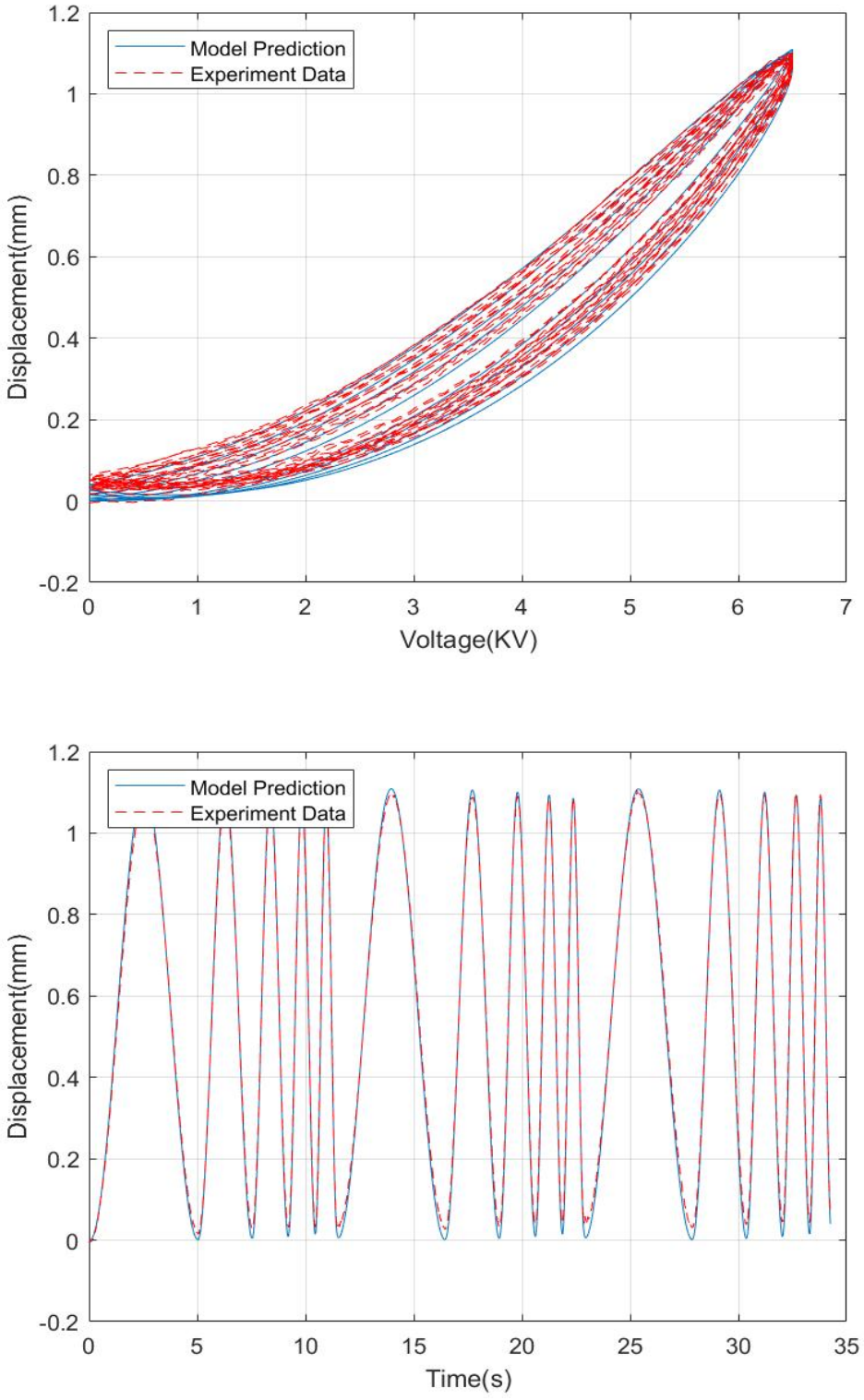

Figure 23: Comparison of model output and experimental result with driving voltage amplitude 6.5kv.

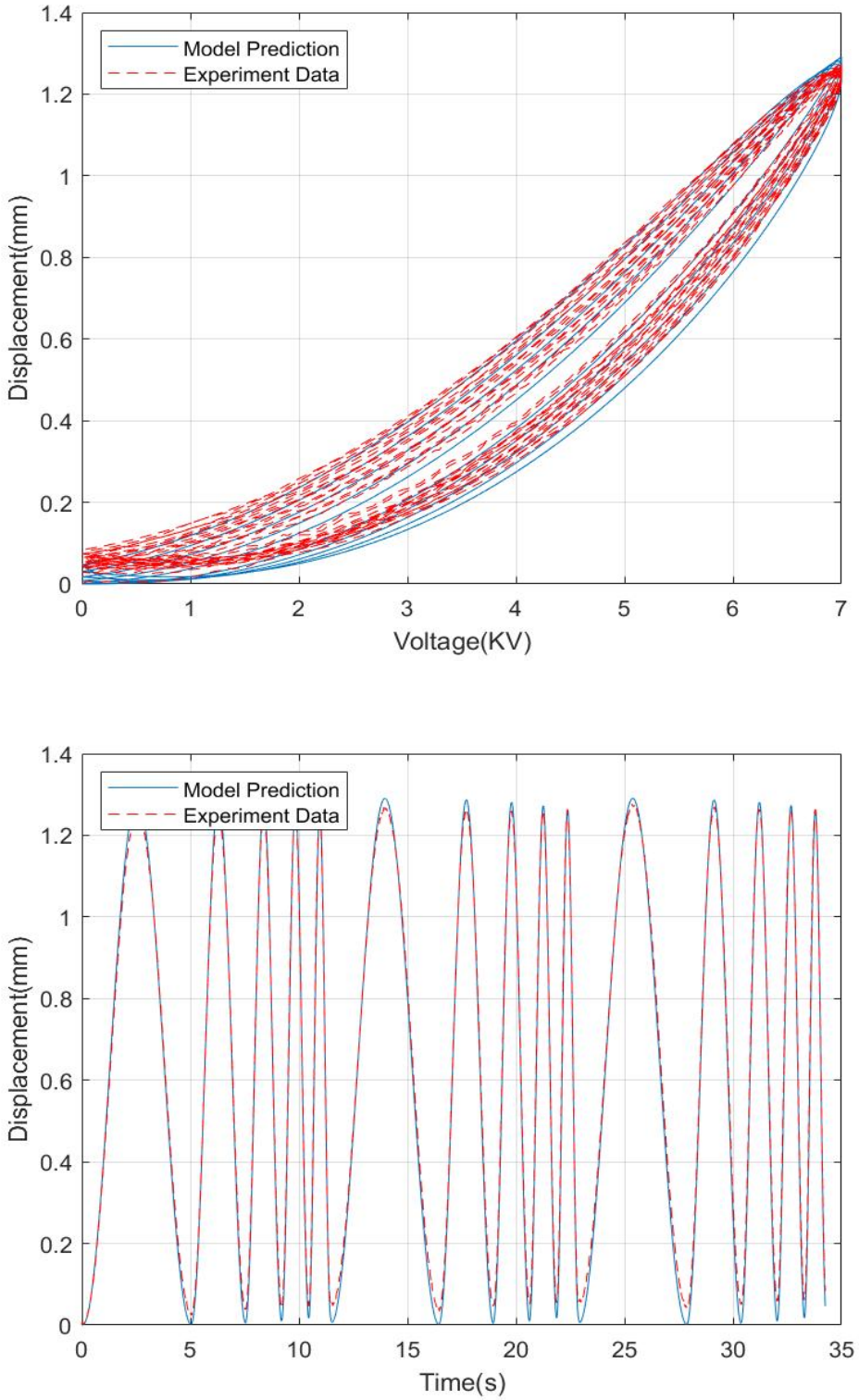

Figure 24: Comparison of model output and experimental result with driving voltage amplitude 7kv.

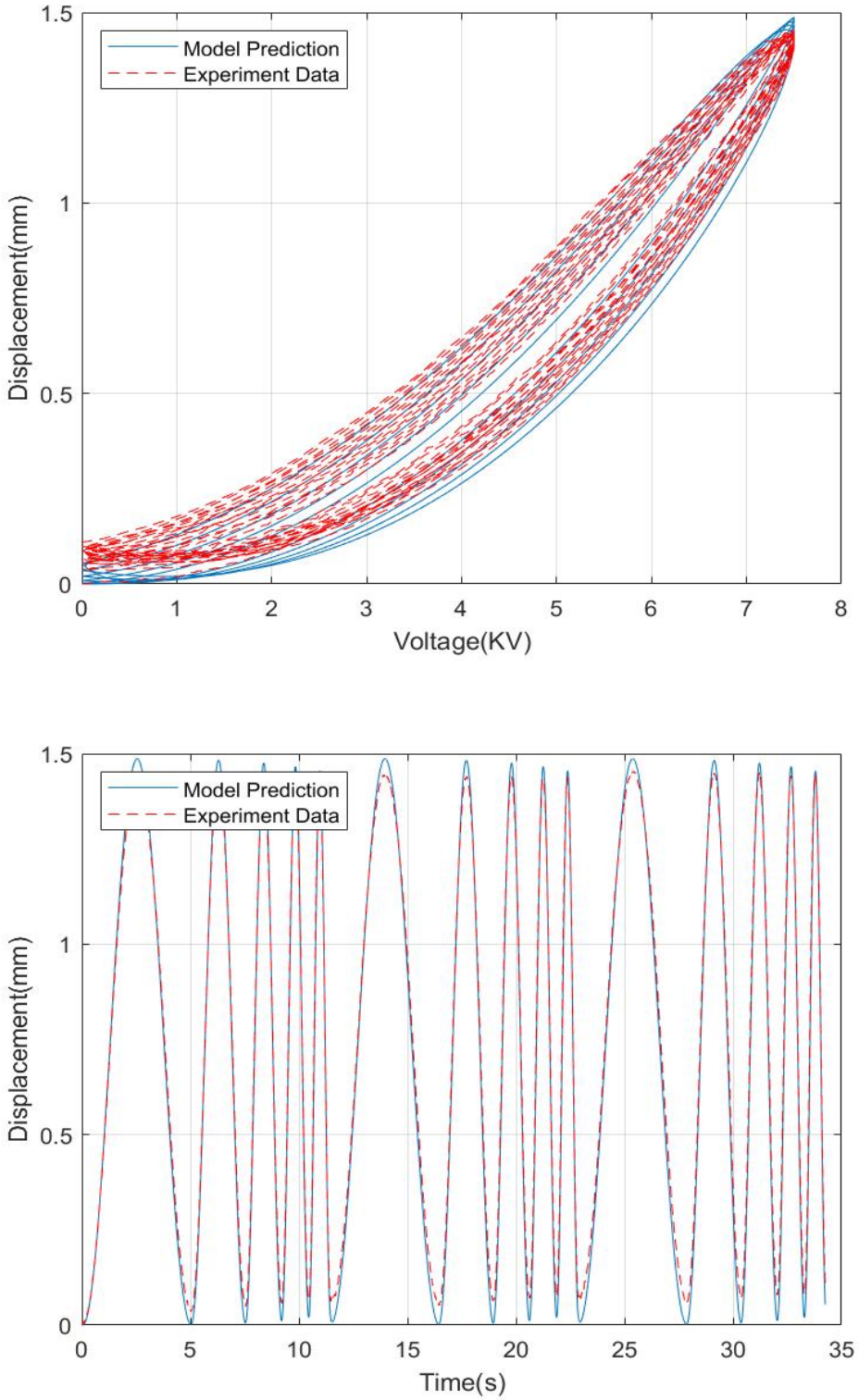

Figure 25: Comparison of model output and experimental result with driving voltage amplitude 7.5kv.

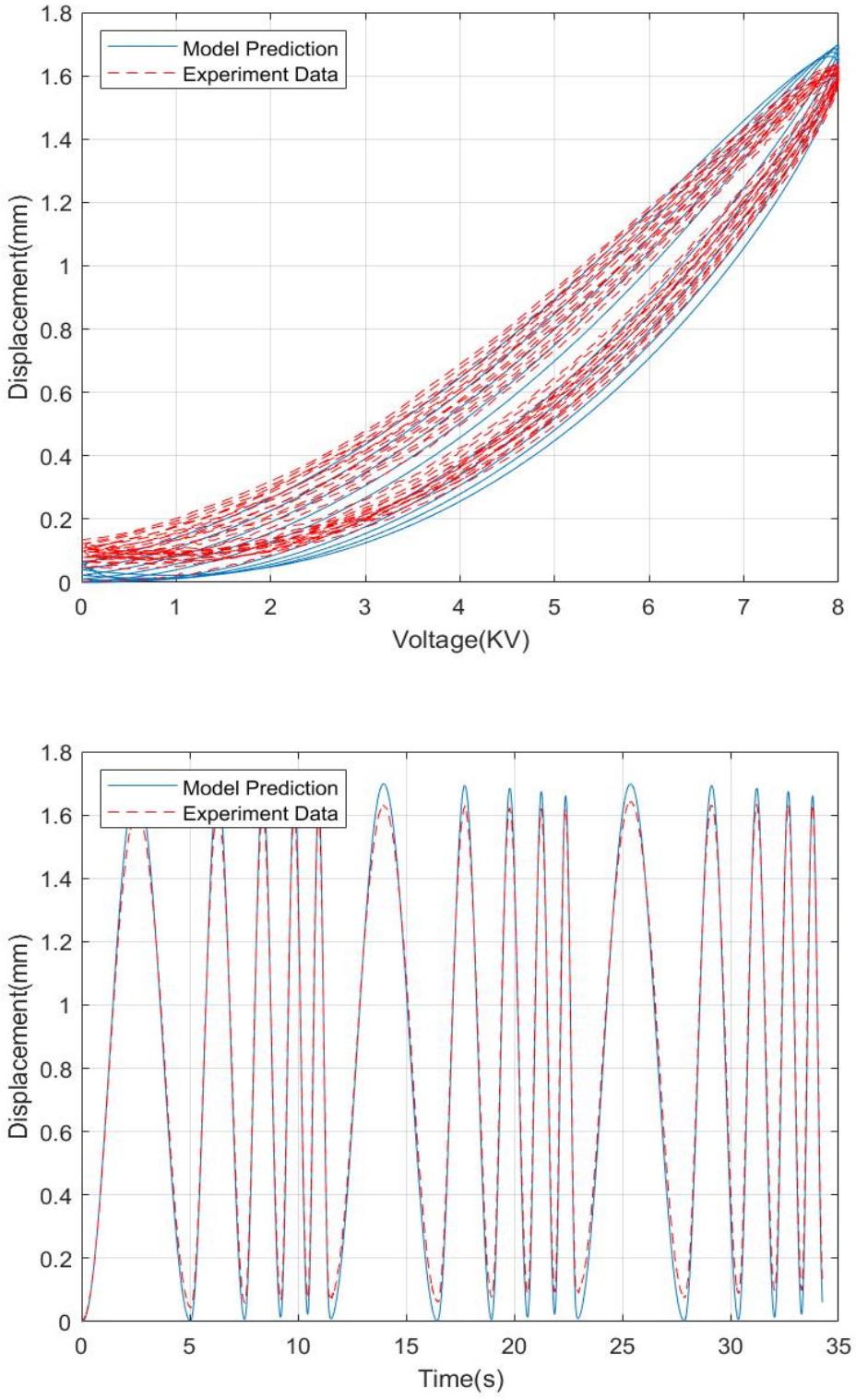

Figure 26: Comparison of model output and experimental result with driving voltage amplitude 8kv.

Chapter 5

Conclude all results and future works

5.1 Conclusions

This paper presented a physics-based dynamic model for a dielectric elastomer actuator (DEA) with a conical shape. The dynamic model relates the voltage provided to the electrodes to the vertical displacement of the center. Firstly, to describe electromechanical coupling of DEA, a dynamic description of the the elastic energy was obtained based on the theory of nonequilibrium thermodynamics. Then a combination of Gent model with Generalized Kelvin element are employed to describe the elastic energy and viscoelasticity, respectively. Secondly, the undetermined parameters in the dynamic model of the DEA are identified by using the differential evolution algorithm. Finally, two-step technique was used to verify the presented dynamic model, by comparing the experimental result and the model prediction output for different input frequencies and amplitudes, respectively. The result demonstrated that the proposed dynamic model can describe the complex nonlinear characteristics and time dependent viscoelastic behavior of the conical DEA. Therefore, the proposed model can effectively describe the nonlinear behaviours and the complex motion characteristics of the conical DEA.

5.2 Future works

In this study, assumed that the DEA is homogeneous in radial direction. However, the inhomogeneous behavior of DEA was observed during experiment, which lead to more nonlinear behavior. Therefore, in future work, to accurately predict the DEA motion, we need to consider the inhomogeneousity. Also, during the experiments a large amount of hystersis and creep was observed, which needs to considered in future studies to have a more precise model.

Furthermore, in the developed model the DEA only has one degree of freedom in vertical direction. However, when the operating environment becomes complicated, DEA should have more directions of motion (more degrees of freedom). Thus, based on the research conducted on this paper, we plan to further study the DEA with multi-directions of motion in the future.

Bibliography

[1] Roy D Kornbluh, Ron Pelrine, Qibing Pei, Richard Heydt, Scott Stanford, Seajin Oh, and Joseph Eckerle. Electroelastomers: applications of dielectric elastomer transducers for actuation, generation, and smart structures. In *Smart structures and materials 2002: Industrial and commercial applications of smart structures technologies*, volume 4698, pages 254–270. International society for optics and photonics, 2002.

[2] Peng Huang, Wenjun Ye, and Yawu Wang. Dynamic modeling of dielectric elastomer actuator with conical shape. *Plos one*, 15(8):e0235229, 2020.

[3] Guo-Ying A2Gu, Jian Zhu, Li-Min Zhu, and Xiangyang Zhu. A survey on dielectric elastomer actuators for soft robots. *Bioinspiration & biomimetics*, 12(1):011003, 2017.

[4] Daniela Rus and Michael T Tolley. Design, fabrication and control of soft robots. *Nature*, 521(7553):467–475, 2015.

[5] Cecilia Laschi and Matteo Cianchetti. Soft robotics: new perspectives for robot bodyware and control. *Frontiers in bioengineering and biotechnology*, 2:3, 2014.

[6] Carmel Majidi. Soft robotics: a perspective—current trends and prospects for the future. *Soft robotics*, 1(1):5–11, 2014.

[7] Invertebrate locomotor systems.

[8] Martin Hülse, Steffen Wischmann, and Frank Pasemann. The role of non-linearity for evolved multifunctional robot behavior. In *International conference on evolvable systems*, pages 108–118. Springer, 2005.

[9] Markus Grebenstein, Maxime Chalon, Werner Friedl, Sami Haddadin, Thomas Wimböck, Gerd Hirzinger, and Roland Siegwart. The hand of the dlr hand arm system: Designed for interaction. *The international journal of robotics research*, 31(13):1531–1555, 2012.

[10] Rolf Pfeifer, Max Lungarella, and Fumiya Iida. The challenges ahead for bio-inspired'soft'robotics. *Communications of the ACM*, 55(11):76–87, 2012.

[11] Sangbae Kim, Cecilia Laschi, and Barry Trimmer. Soft robotics: a bioinspired evolution in robotics. *Trends in biotechnology*, 31(5):287–294, 2013.

[12] L Margheri, C Laschi, and B Mazzolai. Soft robotic arm inspired by the octopus: I. from biological functions to artificial requirements. *Bioinspiration & biomimetics*, 7(2):025004, 2012.

[13] Graham Robinson and J Bruce C Davies. Continuum robots-a state of the art. In *Proceedings 1999 IEEE international conference on robotics and automation (Cat. No. 99CH36288C)*, volume 4, pages 2849–2854. IEEE, 1999.

[14] Deepak Trivedi, Christopher D Rahn, William M Kier, and Ian D Walker. Soft robotics: Biological inspiration, state of the art, and future research. *Applied bionics and biomechanics*, 5(3):99–117, 2008.

[15] Xuanhe Zhao. Multi-scale multi-mechanism design of tough hydrogels: building dissipation into stretchy networks. *Soft matter*, 10(5):672–687, 2014.

[16] Yoseph Bar-Cohen et al. Electroactive polymer actuators as artificial muscles. *SPIE, Washington*, 2001.

[17] Gordon G Wallace, Peter R Teasdale, Geoffrey M Spinks, and Leon AP Kane-Maguire. *Conductive electroactive polymers: intelligent polymer systems*. CRC press, 2008.

[18] Ailish O'Halloran, Fergal O'malley, and Peter McHugh. A review on dielectric elastomer actuators, technology, applications, and challenges. *Journal of applied physics*, 104(7):9, 2008.

[19] Nadia G Cheng, Arvind Gopinath, Lifeng Wang, Karl Iagnemma, and Anette E Hosoi. Thermally tunable, self-healing composites for soft robotic applications. *Macromolecular materials and engineering*, 299(11):1279–1284, 2014.

[20] Zhigang Suo. Theory of dielectric elastomers. *Acta mechanica solida sinica*, 23(6):549–578, 2010.

[21] QM Zhang, J Su, Chy Hyung Kim, R Ting, and Rodger Capps. An experimental investigation of electromechanical responses in a polyurethane elastomer. *Journal of applied physics*, 81(6):2770–2776, 1997.

[22] Guggi Kofod, Werner Wirges, Mika Paajanen, and Siegfried Bauer. Energy minimization for self-organized structure formation and actuation. *Applied physics letters*, 90(8):081916, 2007.

[23] Federico Carpi and Danilo De Rossi. Eyeball pseudo-muscular actuators for an android face. In *Smart structures and materials 2005: Electroactive polymer actuators and devices (eapad)*, volume 5759, pages 16–21. International society for optics and photonics, 2005.

[24] Federico Carpi and Danilo De Rossi. Bioinspired actuation of the eyeballs of an android robotic face: concept and preliminary investigations. *Bioinspiration & biomimetics*, 2(2):S50, 2007.

[25] Ujjaval Gupta, Yuzhe Wang, Hongliang Ren, and Jian Zhu. Dynamic modeling and feedforward control of jaw movements driven by viscoelastic artificial muscles. *IEEE/ASME transactions on mechatronics*, 24(1):25–35, 2018.

[26] Matthias Kollosche, Jian Zhu, Zhigang Suo, and Guggi Kofod. Complex interplay of nonlinear processes in dielectric elastomers. *Physical Review E*, 85(5):051801, 2012.

[27] Manuel Aschwanden and Andreas Stemmer. Low voltage, highly tunable diffraction grating based on dielectric elastomer actuators. In *electroactive polymer actuators and devices 2007*, volume 6524, page 65241N. International Society for Optics and Photonics, 2007.

[28] Sebastian Döring, Matthias Kollosche, Torsten Rabe, Joachim Stumpe, and Guggi Kofod. Electrically tunable polymer dfb laser. *Advanced materials*, 23(37):4265–4269, 2011.

[29] Christoph Keplinger, Jeong-Yun Sun, Choon Chiang Foo, Philipp Rothemund, George M Whitesides, and Zhigang Suo. Stretchable, transparent, ionic conductors. *Science*, 341(6149):984–987, 2013.

[30] Anders Lei, Ruichao Xu, Anders Thyssen, Adam Carsten Stoot, Thomas Lehrmann Christiansen, K Hansen, R Lou-Moeller, Erik Vilain Thomsen, and Karen Birkelund. Mems-based thick film pzt vibrational energy harvester. In *2011 IEEE 24th international conference on micro electro mechanical systems*, pages 125–128. IEEE, 2011.

[31] Karsten Ahnert, Markus Abel, Matthias Kollosche, Per Jørgen Jørgensen, and Guggi Kofod. Soft capacitors for wave energy harvesting. *Journal of materials chemistry*, 21(38):14492–14497, 2011.

[32] Thomas G McKay, Benjamin M O'Brien, Emilio P Calius, and Iain A Anderson. Soft generators using dielectric elastomers. *Applied physics letters*, 98(14):142903, 2011.

[33] Alison Perry, Karen Anderson, Ruth Lean, and Susan Cotton. Elevation of the soft palate in speech and swallowing in normal female participants and females with motor neuron disease: an innovative procedure for measuring palatal elevation. *International journal of language & communication disorders*, 37(2):197–214, 2002.

[34] Iain A Anderson, Todd A Gisby, Thomas G McKay, Benjamin M O'Brien, and Emilio P Calius. Multi-functional dielectric elastomer artificial muscles for soft and smart machines. *Journal of applied physics*, 112(4):041101, 2012.

[35] Na Ni and Ling Zhang. Dielectric elastomer sensors. *Elastomers; Çankaya, N., Ed.; IntechOpen: Rijeka, Croatia*, pages 231–253, 2017.

[36] Yanjun Zheng, Yilong Li, Kun Dai, Yan Wang, Guoqiang Zheng, Chuntai Liu, and Changyu Shen. A highly stretchable and stable strain sensor based on hybrid

carbon nanofillers/polydimethylsiloxane conductive composites for large human motions monitoring. *Composites science and technology*, 156:276–286, 2018.

[37] Paul Brochu and Qibing Pei. Dielectric elastomers for actuators and artificial muscles. *Electroactivity in polymeric materials*, pages 1–56, 2012.

[38] Federico Carpi and Danilo De Rossi. Dielectric elastomer cylindrical actuators: electromechanical modelling and experimental evaluation. *Materials science and engineering: C*, 24(4):555–562, 2004.

[39] Andrew T Conn and Jonathan Rossiter. Towards holonomic electro-elastomer actuators with six degrees of freedom. *Smart materials and structures*, 21(3):035012, 2012.

[40] Nakhiah Goulbourne, Mary I Frecker, Eric Michael Mockensturm, and Alan J Snyder. Modeling of a dielectric elastomer diaphragm for a prosthetic blood pump. In *Smart structures and materials 2003: Electroactive polymer actuators and devices*, volume 5051, pages 319–331. International Society for Optics and Photonics, 2003.

[41] M Babič, R Vertechy, Giovanni Berselli, J Lenarčič, V Parenti Castelli, and G Vassura. An electronic driver for improving the open and closed loop electromechanical response of dielectric elastomer actuators. *Mechatronics*, 20(2):201–212, 2010.

[42] M Follador, F Tramacere, and B Mazzolai. Dielectric elastomer actuators for octopus inspired suction cups. *Bioinspiration & biomimetics*, 9(4):046002, 2014.

[43] Shi Cheng and Zhigang Wu. Microfluidic electronics. *Lab on a chip*, 12(16):2782–2791, 2012.

[44] Kwangmok Jung, Ja Choon Koo, Young Kwan Lee, Hyouk Ryeol Choi, et al. Artificial annelid robot driven by soft actuators. *Bioinspiration & biomimetics*, 2(2):S42, 2007.

[45] F Carpi and D De Rossi. Contractile folded dielectric elastomer actuators. In *Electroactive polymer actuators and devices 2007*, volume 6524, page 65240D. International Society for Optics and Photonics, 2007.

[46] Marc Matysek, Henry Haus, Holger Moessinger, Dirk Brokken, Peter Lotz, and Helmut F Schlaak. Combined driving and sensing circuitry for dielectric elastomer actuators in mobile applications. In *electroactive polymer actuators and devices 2011*, volume 7976, page 797612. International Society for Optics and Photonics, 2011.

[47] Chongjing Cao and Andrew T Conn. Performance optimization of a conical dielectric elastomer actuator. In *Actuators*, volume 7, page 32. Multidisciplinary Digital Publishing Institute, 2018.

[48] Huai Xiao, Jundong Wu, Wenjun Ye, and Yawu Wang. Dynamic modeling of dielectric elastomer actuators based on thermodynamic theory. *Mechanics of advanced materials and structures*, pages 1–10, 2020.

[49] Guo-Ying Gu, Ujjaval Gupta, Jian Zhu, Li-Min Zhu, and Xiangyang Zhu. Modeling of viscoelastic electromechanical behavior in a soft dielectric elastomer actuator. *IEEE transactions on robotics*, 33(5):1263–1271, 2017.

[50] Eduard Benet and Franck J Vernerey. Dynamic competition of inflation and delamination in the finite deformation of thin membranes. *Soft matter*, 15(33):6630–6641, 2019.

[51] Xunuo Cao, Mingqi Zhang, Zhen Zhang, Yi Xu, Youhua Xiao, and Tiefeng Li. Review of soft linear actuator and the design of a dielectric elastomer linear actuator. *Acta mechanica solida sinica*, 32(5):566–579, 2019.

[52] Tianhu He, Leilei Cui, Cheng Chen, and Zhigang Suo. Nonlinear deformation analysis of a dielectric elastomer membrane–spring system. *Smart materials and structures*, 19(8):085017, 2010.

[53] HM Wang. Viscoelastic analysis of a spring-connected dielectric elastomer actuator undergoing large inhomogeneous deformation. *International journal of mechanical sciences*, 136:17–23, 2018.

[54] Ronald E Pelrine, Roy D Kornbluh, and Jose P Joseph. Electrostriction of polymer dielectrics with compliant electrodes as a means of actuation. *Sensors and actuators : Physical*, 64(1):77–85, 1998.

[55] Guggi Kofod. Dielectric elastomer actuators. *Chemistry*, 2001.

[56] Feng-bo Zhu, Chun-li Zhang, Jin Qian, and Wei-qiu Chen. Mechanics of dielectric elastomers: materials, structures, and devices. *Journal of Zhejiang University-science A*, 17(1):1–21, 2016.

[57] Ron Pelrine, Roy Kornbluh, Qibing Pei, and Jose Joseph. High-speed electrically actuated elastomers with strain greater than 100%. *Science*, 287(5454):836–839, 2000.

[58] Liwu Liu, Yanju Liu, Jinsong Leng, and Kin-tak Lau. Electromechanical stability of compressible dielectric elastomer actuators. *Smart materials and structures*, 20(11):115015, 2011.

[59] Raymond William Ogden. Large deformation isotropic elasticity–on the correlation of theory and experiment for incompressible rubberlike solids. *Proceedings of the royal society of London. Mathematical and physical sciences*, 326(1567):565–584, 1972.

[60] Alan N Gent. A new constitutive relation for rubber. *Rubber chemistry and technology*, 69(1):59–61, 1996.

[61] XinJiang Lu, YanKun Lin, and TeTe Hu. Physic-based and control-oriented modeling based robust control for soft dielectric elastomer actuator. *Smart materials and structures*, 29(3):035026, 2020.

[62] Matthias Kollosche, Guggi Kofod, Zhigang Suo, and Jian Zhu. Temporal evolution and instability in a viscoelastic dielectric elastomer. *Journal of the mechanics and physics of solids*, 76:47–64, 2015.

[63] Jianyou Zhou, Liying Jiang, and Roger E Khayat. Investigation on the performance of a viscoelastic dielectric elastomer membrane generator. *Soft matter*, 11(15):2983–2992, 2015.

[64] Jianping Gu, Zhimin Xie, Shaoxiang Wang, Huiyu Sun, and Xiaopeng Zhang. Thermo-mechanical modeling of woven fabric reinforced shape memory polymer composites. *Mechanics of advanced materials and structures*, 26(12):1042–1052, 2019.

[65] Katherine Acton and Brian Weick. Orthotropic viscoelastic behavior of polymer tape in a wound roll. *Mechanics of advanced materials and structures*, 21(1):53–66, 2014.

[66] Jung-Hwan Youn, Seung Mo Jeong, Geonwoo Hwang, Hyunwoo Kim, Kyujin Hyeon, Jihwan Park, and Ki-Uk Kyung. Dielectric elastomer actuator for soft robotics applications and challenges. *Applied sciences*, 10(2):640, 2020.

[67] Wei Hong. Modeling viscoelastic dielectrics. *Journal of the mechanics and physics of solids*, 59(3):637–650, 2011.

[68] Zezhou Li, Lei Qin, Dongsheng Zhang, Aifen Tian, Henry YK Lau, and Ujjaval Gupta. Modeling and feedforward control of a soft viscoelastic actuator with inhomogeneous deformation. *Extreme mechanics letters*, 40:100881, 2020.

[69] A Serra-Aguila, JM Puigoriol-Forcada, G Reyes, and J Menacho. Viscoelastic models revisited: Characteristics and interconversion formulas for generalized kelvin–voigt and maxwell models. *Acta mechanica sinica*, 35(6):1191–1209, 2019.